Journal of Geochemical Exploration 258 (2024) 107419

Contents lists available at ScienceDirect

Journal of Geochemical Exploration

journal homepage: www.elsevier.com/locate/gexplo

U-Pb geochronology, tourmaline geochemistry, and stable (B, S) isotope constraints from the Hirvilavanmaa Au-only and the polymetallic Naakenavaara orogenic gold deposits, Central Lapland belt, northern Finland

Mikael Vasilopoulos [a,*,1], Ferenc Molnár [b], Jukka-Pekka Ranta [a], Matti Kurhila [c], Hugh O'Brien [c], Yann Lahaye [c], Sari Lukkari [c], Marko Moilanen [a]

[a] Oulu Mining School, University of Oulu, P.O. Box 3000, 90014 Oulu, Finland
[b] Institute of Geography and Geosciences, Eötvös Loránd University, Pázmány Péter s. 1/C, 1117 Budapest, Hungary
[c] Geological Survey of Finland, P.O. Box 96, FI-02151 Espoo, Finland

ARTICLE INFO

Keywords:
Monazite
Xenotime
Tourmaline
Orogenic gold
Sulfur isotopes
Boron isotopes

ABSTRACT

In this study of the Hirvilavanmaa Au-only and the polymetallic (Au-Cu-Co-Ni) Naakenavaara orogenic gold deposits from the Central Lapland belt (CLB) we present precise U-Pb ages obtained by single collector LA-ICP-MS from hydrothermal monazite and xenotime associated with different stages of hydrothermal activity in the deposits. We also use crystal chemical data from tourmaline, and in situ sulfur isotopes from sulfides, and boron isotope data from tourmaline obtained by LA-MC-ICP-MS to study sources of ore-forming components and conditions during ore deposition. Ages of texturally and paragenetically constrained hydrothermal xenotime indicate that Co deposition (1816 ± 10 Ma) and subsequent Cu deposition (1804 ± 3.3 Ma) at Naakenavaara took place during deformation events at ca. 1.82–1.80 Ga, and that ore-related hydrothermal activity had also begun at Hirvilavanmaa (1822 ± 9 Ma) during the same events, which can be related to late-orogenic Svecofennian tectonism and deformation in the CLB. Hydrothermal activity that led to Au deposition in both deposits took place during the waning stages of the Svecofennian orogeny, with hydrothermal monazite giving ages of 1785 ± 10 Ma and 1752 ± 10 Ma for Hirvilavanmaa and Naakenavaara, respectively. Tourmaline crystal chemistry indicates low fluid/rock ratios during tourmaline deposition in both deposits, with relatively oxidizing conditions during ore formation at Hirvilavanmaa and during the early Co-rich mineralizing stage at Naakenavaara but more reducing conditions for the subsequent Cu-rich mineralizing stage at Naakenavaara. Sulfur and boron-isotope compositions of sulfide minerals and tourmaline, respectively, point towards a mafic metavolcanic rock source for the ore-forming components at Hirvilavanmaa, and a metasedimentary source at Naakenavaara. There has only been limited previous work on the precise dating of mineralizing stages and on the sources of ore-forming components in individual orogenic deposits in the CLB. Results from our study provide important constraints on the timing of hydrothermal mineralization and different sources of ore-forming components in both Au-only and base metal-rich orogenic deposits in the CLB, one of the most important metallogenic belts in the Fennoscandian Shield with significant potential for new discoveries.

1. Introduction

The Paleoproterozoic Central Lapland belt (CLB; formerly known as Central Lapland Greenstone Belt) in northern Finland is one of the most important precious and base metal metallogenic belts in the Fennoscandian Shield, yet it has a relatively short exploration history and significant potential for new discoveries (Niiranen et al., 2015; Eilu et al., 2015). One of the most significant mineral deposit types in the CLB is orogenic gold, a common ore type in Precambrian greenstone belts in Finland and globally (Eilu et al., 2007, 2012; Eilu, 2015; Wyche et al.,

* Corresponding author.
E-mail address: mikael.vasilopoulos@gtk.fi (M. Vasilopoulos).
[1] Current address: Geological Survey of Finland, P.O. Box 96, FI-02151 Espoo, Finland.

https://doi.org/10.1016/j.gexplo.2024.107419
Received 8 March 2023; Received in revised form 27 December 2023; Accepted 1 February 2024
Available online 5 February 2024

2015; Fig. 1a). Approximately half of all known occurrences of orogenic gold in the CLB, are also significantly enriched in Cu ± Co ± Ni in addition to Au. These polymetallic deposits have been classified as orogenic Au deposits with atypical metal association (e.g., Eilu et al., 2007, 2012; Holma and Keinänen, 2007; Holma et al., 2007; Eilu, 2015). The majority of the orogenic Au occurrences in the CLB, including most of the polymetallic ones, are spatially associated with the east-west trending Sirkka Shear Zone (SiSZ) and its subsidiary shear and fault zones (Eilu et al., 2007; Fig. 1a). A second significant structure in the CLB is the NNE-trending Kiistala Shear Zone (KiSZ), which hosts the Suurikuusikko deposit, currently the largest Au producer in Europe (approximately 200 koz of Au produced annually; Agnico Eagle, 2023), along with other Au-only deposits (Fig. 1a).

The sources of metals, ligands and fluids leading to formation of classic orogenic Au deposits, are still subjects of debate (e.g., Goldfarb and Groves, 2015; Groves et al., 2020; Goldfarb and Pitcairn, 2022). However, several workers have suggested metamorphic devolatilization as a key process leading to generation of ore-forming fluids and formation of orogenic Au deposits in Precambrian greenstone belts (Phillips and Powell, 2010; Zhong et al., 2015; Niiranen et al., 2015; Patten et al., 2020; Pitcairn et al., 2021). The genesis of atypical base metal-rich orogenic deposits has been explained by models proposing mobilization of saline basinal fluids under moderate to high-grade metamorphic conditions prior to the orogeny (e.g. Yardley and Graham, 2002; Yardley and Cleverley, 2013; Qiu et al., 2021), and the overprinting of an earlier base metal-rich deposit by later orogenic gold mineralization through the reactivation of the same structures during subsequent events (Groves et al., 2003; Molnár et al., 2018; Vasilopoulos et al., 2021, 2023; Ranta et al., 2021; Raič et al., 2022). Several studies have shown that the sulfur isotope composition of sulfides can provide valuable information regarding the sources of sulfur and the physicochemical conditions during ore formation in various geological environments (e.g., Ohmoto, 1972; Hodkiewicz et al., 2009; Molnár et al., 2016; Vasilopoulos et al., 2021). Tourmaline, on the other hand, is commonly associated with gold deposits (e.g., Goldfarb et al., 2005; Sciuba et al., 2021) and exhibits a high degree of stability after

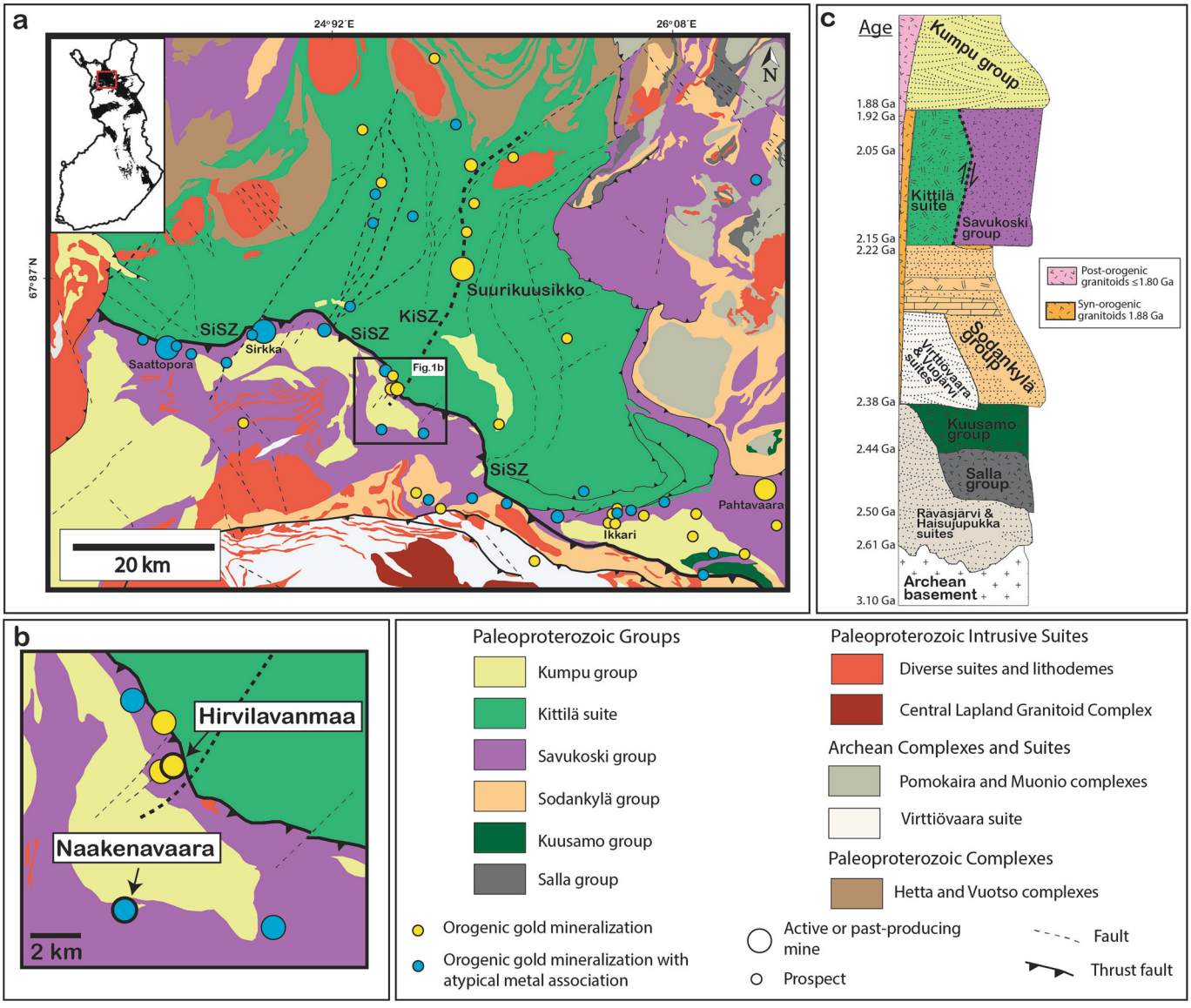

Fig. 1. (a) Simplified geological map of the Central Lapland belt (CLB) showing Au-only (yellow circles) and atypical base metal-rich (blue circles) orogenic Au deposits and occurrences. Inset map of Finland shows position of CLB. Base map modified from the Mineral Deposits and Exploration database of the Geological Survey of Finland (GTK, 2023); information about the depicted deposits and occurrences taken from the same source. (b) Detailed view of marked area from panel a, showing location of Hirvilavanmaa and Naakenavaara deposits. (c) Stratigraphic column of CLB, modified after Köykkä et al. (2019). (For interpretation of the references to colour in this figure legend, the reader is referred to the web version of this article.)

crystallization, making it a useful tool in evaluating the local chemical environment during its formation (van Hinsberg et al., 2011; Molnár et al., 2016: Ranta et al., 2017). Tourmaline is also the major boron sink in hydrothermal systems and, due to the wide range of isotopic fractionation of boron in different geological environments, boron isotope data of tourmaline can be used to constrain the source of boron in hydrothermal systems (e.g., Henry and Dutrow, 1996; Marschall and Jiang, 2011; Trumbull et al., 2020). There are only limited studies available on the sources of ore-forming components in orogenic Au deposits from the CLB (Mänttäri, 1995; Niiranen et al., 2015; Molnár et al., 2017, 2018, 2019; Patten et al., 2020, 2023) and additional detailed studies on individual deposits utilizing geochemical tools such as stable isotopes and crystal chemistry of tourmaline could help to better constrain these sources.

The CLB underwent deformation and metamorphism during the 1.92–1.77 Ga Svecofennian orogeny but the age of metamorphism in the CLB is not well constrained and precise radiometric ages related to the formation of orogenic Au deposits are also limited. Apart from a few texturally well-constrained studies (e.g., Molnár et al., 2017, 2018, 2019), previous geochronological studies have mostly used mineral separates without a direct textural link to different mineralizing stages. Geochronological studies based on a well-established textural context and high resolution in situ analytical techniques (e.g., LA-ICP-MS) have the potential to reveal important information regarding the age of mineralizing stages in both Au-only and atypical orogenic deposits in the CLB. Xenotime and monazite are ideal for precise U-Pb age dating due to their relatively high U and low common Pb concentrations, their high "closure" temperatures, their resistance to chemical alteration, and their ability to crystallize in different geological environments and over a wide range of temperatures (e.g., Cherniak, 2006; Cherniak et al., 2004; Hetherington and Harlov, 2008; Rasmussen et al., 2011; Seydoux-Guillaume et al., 2012; Vielreicher et al., 2015).

This study of the Hirvilavanmaa Au-only and the polymetallic Naakenavaara orogenic gold deposits (Fig. 1b) from the Central Lapland belt builds on a comparative study on the same deposits by Vasilopoulos et al. (2023). Here we utilize the previously-established mineralogical, lithogeochemical and sulfide trace element characteristics of different mineralizing stages in both deposits as a contextual basis for new work. We present U-Pb ages for hydrothermal monazite and xenotime from different mineralization and alteration stages in the deposits using in situ laser ablation inductively coupled mass spectrometry (LA-ICP-MS) and evaluate how these absolute ages relate to the previously-established sequence of mineralizing events. In addition, we present sulfur and boron isotope data obtained by in situ analyses of sulfides and tourmaline, respectively, together with crystal chemical data from tourmaline for better understanding of conditions during ore deposition and sources of ore-forming components.

2. Geological setting

2.1. Geological evolution of the CLB

The CLB of northern Finland is part of a larger Paleoproterozoic greenstone belt extending from northern Norway, through the Finnish Lapland, to Russian Karelia (Hanski and Huhma, 2005). The deposition of supracrustal rocks in the CLB began during the early Paleoproterozoic rifting of the Archaean basement and was terminated by the initiation of the Svecofennian orogeny (ca. 1.92 Ga; Lahtinen et al., 2005; Korja et al., 2006; Köykkä et al., 2019). The stratigraphy of the CLB comprises the Salla, Kuusamo, Sodankylä, Savukoski, and Kumpu groups along with the Kittilä suite and several minor suites and lithodemes (Fig. 1c; Köykkä et al., 2019). The aforementioned lithostratigraphic groups were intruded by 2.44–2.05 Ga mafic-ultramafic layered intrusions and ca. 1.88–1.76 Ga syn- to post-orogenic granitoids (Nironen, 2005; Patison, 2007; Köykkä et al., 2019).

The rift basin stage of evolution (ca 2.5–2.1 Ga) is linked to the breakup of the Kenorland supercontinent and is responsible for the deposition of the Salla and Kuusamo groups that are principally composed of felsic- to intermediate and tholeiitic to komatiitic metavolcanic rocks, respectively. The following syn-rift and syn- to post-rift stages comprise volcanism and sedimentation corresponding to the Sodankylä group (Köykkä et al., 2019). Sodankylä group rocks cover large areas in the CLB (Fig. 1a) and consist of quartzites, mica schists, minor stromatolitic carbonates and mafic metavolcanic rocks. The post-rift stage (ca. 2.1–1.92 Ga) involved the deposition of the Savukoski group and Kittilä suite (Köykkä et al., 2019). The Savukoski group comprises phyllitic metasediments and graphite- and sulfide-bearing black schists intercalated with minor tuffites (Lehtonen et al., 1998), overlain by komatiitic and picritic metavolcanic rocks. The 6–9 km thick allocthonous Kittilä suite represents the largest sequence of mafic volcanic rocks in the Fennoscandian Shield (Hanski and Huhma, 2005) and overlies rocks of the Savukoski group. The Kittilä suite comprises Fe- to Mg-tholeiitic basalts, plagioclase porphyry felsic intrusions, banded iron formations and various metasedimentary packages. The Svecofennian foreland basin stage includes deposition of rocks belonging to the Kumpu group, which is the uppermost major lithological unit of the CLB (Köykkä et al., 2019); it comprises thick metasedimentary packages and syngenetic felsic metavolcanic rocks with their deposition likely occurring after 1.88 Ga (Hanski and Huhma, 2005).

Multiple stages of metamorphism and ductile deformation and a subsequent stage of brittle deformation affected the CLB during the 1.92–1.77 Ga Svecofennian orogeny (Hölttä et al., 2007; Patison, 2007; Lahtinen et al., 2015; Sayab et al., 2020). Sayab et al. (2020) established five stages of deformation for the CLB (D1-D5), and readers are referred to their work for a detailed description of the deformational evolution of the CLB. Most of the discovered orogenic gold deposits in the CLB are hosted in its central part, which is dominated by mafic metavolcanic rocks of the Kittilä suite, surrounded by rocks of the Savukoski, Kumpu, and Sodankylä groups (Fig. 1a). Rocks in the central part of the CLB are characterized by greenschist facies metamorphic grade, and they are bound in all directions by mid-amphibolite facies rocks (Hölttä and Heilimo, 2017). The age of metamorphism in the CLB is not well constrained but the consensus is that metamorphic conditions reached their peak between 1.88 and 1.86 Ga (Lahtinen et al., 2015; Hölttä and Heilimo, 2017). A Re-Os age from arsenopyrite, and modelling done on disturbed Re-Os systems in sulfides from the Suurikuusikko and Iso-Kuotko Au deposits, respectively, indicate that formation of orogenic gold mineralization in the CLB had started during early collision and ductile deformation stages (ca. 1.92–1.88 Ga; Wyche et al., 2015; Molnár et al., 2018). However, the majority of orogenic gold deposits in the CLB formed during late- to post orogenic hydrothermal events (post 1.85 Ga) related to the final stage of brittle deformation (Patison, 2007; Lahtinen et al., 2012; Molnár et al., 2017, 2018, 2019).

2.2. Geology of the Hirvilavanmaa deposit

The Hirvilavanmaa Au-only deposit is a typical orogenic Au-only deposit in the CLB. It is situated in the southern part of the CLB (Fig. 1a–b), approximately 15 km northeast from the town of Kittilä, and is the closest known mineralization to the intersection between the SiSZ and the KiSZ (approximately 0.5 km; Fig. 1a). The gold mineralization at Hirvilavanmaa is mainly hosted by intensely altered and deformed ultramafic metavolcanic rocks of komatiitic affinity that appear as various schists, albite-carbonate-chlorite-sericite rocks, and carbonate rocks (Fig. 2d–f). Early alteration stages that predate Au mineralization started with talc and early, low-degree carbonatization and were followed by albitization (Vasilopoulos et al., 2023). Hulkki and Keinänen (2007) also recognized an early regional chlorite alteration event. These stages were followed by Au mineralization accompanied by abundant quartz-dominant veining, deposition of chlorite and tourmaline in the alteration haloes of the veins, and by late carbonatization (Hulkki and Keinänen, 2007; Vasilopoulos et al., 2023). Gold is mainly hosted as

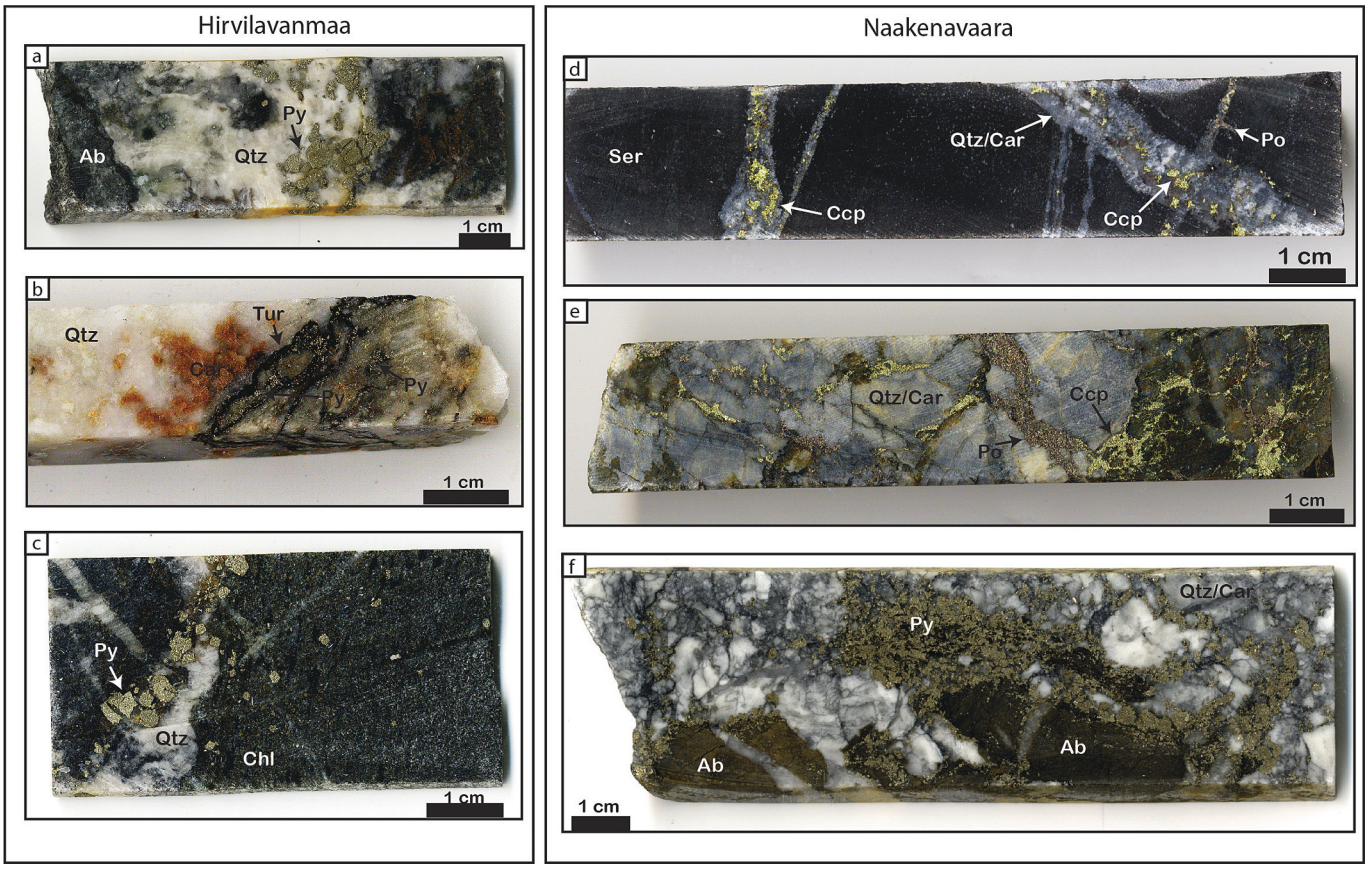

Fig. 2. Representative photographs of wetted drillcore samples of host rocks at Naakenavaara and Hirvilavanmaa. Abbreviations: Ab = albitized host rock, Car = carbonate, Ccp = chalcopyrite, Chl = chlorite-rich host rock, Po = pyrrhotite, Py = pyrite, Qtz = quartz vein, Qtz/Car = quartz- and carbonate-rich vein, Ser = sericite-rich host rock, Tur = tourmaline. (a) Talc-rich part of host rock from Hirvilavanmaa cut by quartz-carbonate vein with pyrite and hematite in the alteration halo. (b) Quartz-carbonate vein from Hirvilavanmaa containing tourmaline- and sulfide-rich slivers of host rock. (c) Albite-talc-chlorite alteration of host rock and different generations of quartz-carbonate veins. Disseminated pyrite is present in the veins and in the alteration haloes around them. (d) Mica schist from Naakenavaara cut by several sulfide-bearing carbonate-quartz veins. Part of a Cu-Au ore zone. (e) Part of Cu-Au ore zone from Naakenavaara: quartz-carbonate vein with abundant chalcopyrite and pyrrhotite. (f) Thick carbonate-quartz vein brecciating albitized host rock from Naakenavaara; vein contains abundant pyrite. Part of a Co ore zone. Photographs are modified from Vasilopoulos et al. (2023).

inclusions and fracture fillings in pyrite within the quartz-carbonate veins and their chlorite-rich alteration haloes (Fig. 3a–c; Vasilopoulos et al., 2023). Pyrite overwhelmingly dominates the sulfide mineralogy of the deposit, and hematite, magnetite and chalcopyrite are common accessory minerals. At Hirvilavanmaa, the multi-stage evolution of the deposit is reflected by the presence of three pyrite generations (Py_{Hirvi}-1, Py_{Hirvi}-2, and Py_{Hirvi}-3 from oldest to youngest) with moderately different Co/Ni ratios but otherwise similar trace element characteristics (Vasilopoulos et al., 2023). According to Hulkki and Keinänen (2007) the Au mineralization formed late in the structural history of the CLB, and it postdates regional peak metamorphism. Recent drilling has indicated that the mineralized zone extends both vertically and horizontally beyond the previously known limits of 270 m in length and 90 m in width, remaining open at depth and along strike to the north (Rupert Resources, 2020). For a more detailed account of lithological, mineralogical, and geochemical characteristics and information related to the exploration history of the Hirvilavanmaa deposit the reader is referred to Vasilopoulos et al. (2023).

2.3. Geology of the Naakenavaara deposit

The polymetallic Naakenavaara deposit is situated just over 5 km SSW from Hirvilavanmaa (Fig. 1a–b) and is an example of an atypical base metal (Cu, Co, Ni) -rich orogenic Au deposit in the CLB (Nenonen, 1975; Taranis Resources, 2010, 2011; Vasilopoulos et al., 2023). The deposit is mainly hosted by altered phyllites and sericite schists (Fig. 2a–c) with comparatively minor amounts of mafic and ultramafic metavolcanic rocks also present in the host sequence (Nenonen, 1975; Keinänen, 2002; Vasilopoulos et al., 2023). The deposit hosts Cu concentrations up to 2.3 wt% and is also enriched in Co, Au, and Ni (concentrations up to 0.1 wt% for Co and Ni and up to 10.3 ppm for Au; Vasilopoulos et al., 2023). The precise extent of the mineralized zones has not been defined yet (Nenonen, 1975; Keinänen, 2002; Taranis Resources, 2014). Pre-ore albitization was followed by alteration events that produced abundant sericite, chlorite, biotite, and carbonate minerals. The ore at Naakenavaara comprises sulfide minerals occuring principally within quartz-carbonate veins and subordinately as fine dissemination in the wall rocks surrounding them (Vasilopoulos et al., 2023). The main type of ore at Naakenavaara is characterized by Cu (±Au) enrichment, with Cu being the most significantly enriched metal in the deposit. Less widespread zones of Co (±Au) enrichment mark the second type of ore; overlapping zones of Cu-Co enrichment are also locally present (Vasilopoulos et al., 2023). The first mineralizing event started as Co-rich and developed into the main Cu-rich stage. The early Co-rich mineralizing stage deposited pyrite with intermediate Co/Ni ratios (Py_{Naak}-mid), before evolving into the main Cu-rich stage that deposited abundant chalcopyrite, pyrrhotite, and pyrite with high Co/Ni ratios (Py_{Naak}-high) in quartz-carbonate veins (Vasilopoulos et al., 2023; Fig. 3g–i). A late orogenic Au event locally overprinted Cu and Co ore zones, depositing Au together with pyrite, pyrrhotite and chalcopyrite in

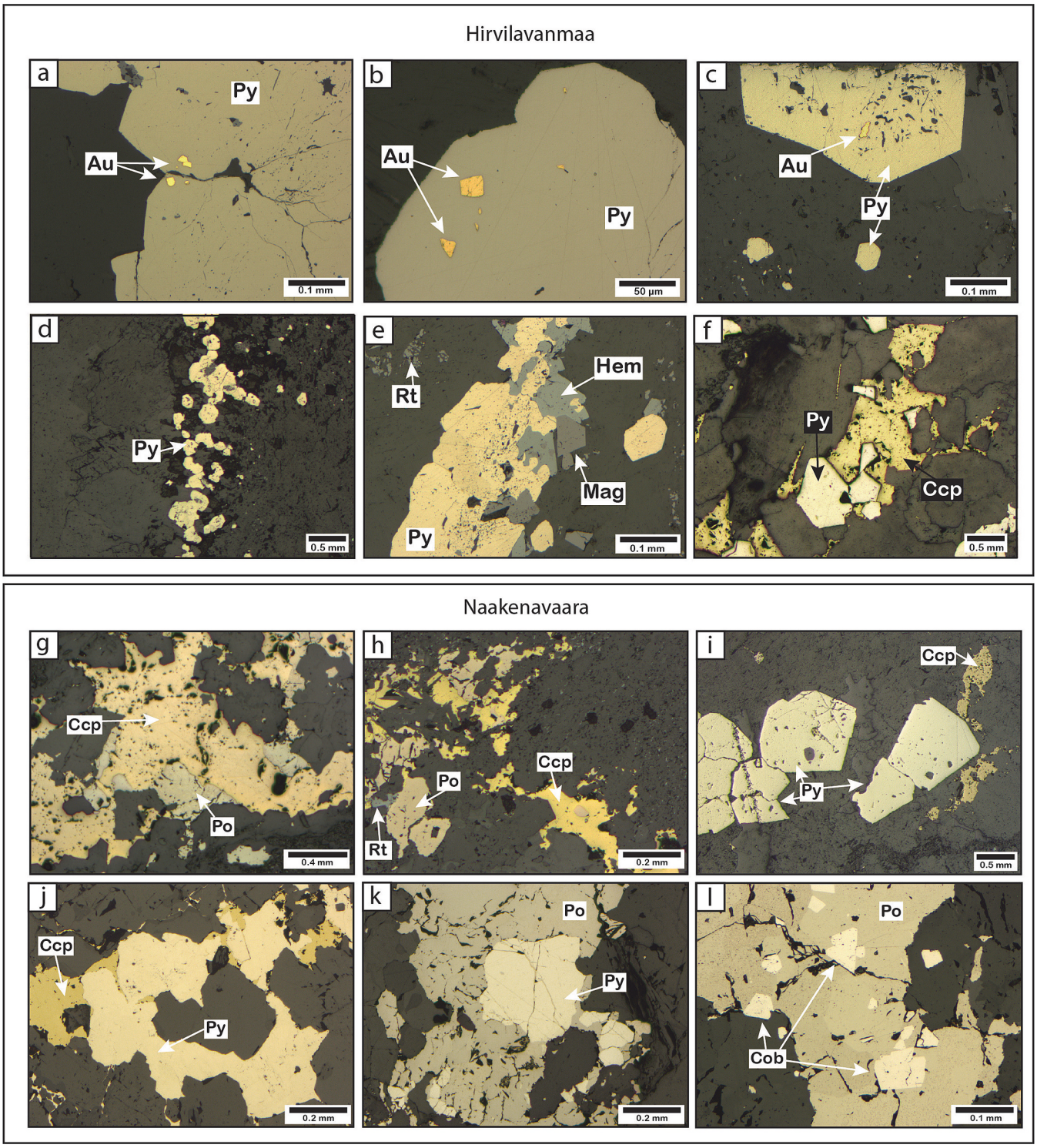

Fig. 3. Photomicrographs in reflected light of Hirvilavanmaa and Naakenavaara samples depicting representative examples of sulfides. For Hirvilavanmaa, pyrite generations are distinguished mainly based on their chemical composition. Inclusion-rich cores belong mostly to Py_{Hirvi}-1, whereas rims belong to Py_{Hirvi}-2 or Py_{Hirvi}-3. For Naakenavaara, the pyrite generations are mentioned in the relevant captions. For more information regarding the characteristics of each pyrite generation in the deposits the reader is referred to Vasilopoulos et al. (2023). Abbreviations: Au = native Au, Ccp = chalcopyrite, Hem = hematite, Mag = magnetite, Po = pyrrhotite, Py = pyrite, Rt = rutile. (a) Pyrite grain aggregate with native Au inclusions from Hirvilavanmaa. (b) Pyrite from Hirvilavanmaa with native Au inclusions. (c) Disseminated pyrite from Hirvilavanmaa. The largest pyrite contains abundant silicate mineral inclusions in the core together with a relatively large native Au inclusion. (d) Disseminated pyrite from Hirvilavanmaa forming individual grains and grain aggregates. (e) Pyrite closely associated with hematite and magnetite. (f) Pyrite and chalcopyrite from Hirvilavanmaa in a mixed sulfide patch. (g) Chalcopyrite-pyrrhotite patch from a Cu-rich zone from Naakenavaara. (h) Patchy chalcopyrite and pyrrhotite from a Cu-rich sample from Naakenavaara. (i) Euhedral pyrite (Py_{Naak}-mid) together with minor chalcopyrite in a Co-rich sample from Naakenavaara. (j) Pyrite (Py_{Naak}-low)-chalcopyrite mixed sulfide patch from a late carbonate-quartz vein from Naakenavaara. (k) Anhedral pyrite (Py_{Naak}-high) intergrown with pyrrhotite; part of a Cu-rich sample from Naakenavaara. (l) Cobaltite inclusions in pyrrhotite; part of a Co-rich sample. Figure modified after Vasilopoulos et al. (2023).

carbonate-rich quartz-carbonate veins. Pyrite (Py_{Naak}-low) deposited during the late Au-rich overprinting has low Co/Ni ratios and generally distinct trace element characteristics compared to the other pyrite types, with differences in the concentration of As and W reaching several orders of magnitude (Vasilopoulos et al., 2023). For a more detailed account of lithological, mineralogical, and geochemical characteristics and information related to the exploration history of the Naakenavaara deposit the reader is referred to Vasilopoulos et al. (2023).

3. Sampling and study methods

This study utilizes the same samples characterized by Vasilopoulos et al. (2023). Sulfur isotope analyses from sulfide minerals, tourmaline boron isotope analyses, and U-Pb dating of monazite and xenotime were all done at the Finnish Geosciences Research Laboratories, Geological Survey of Finland (GTK). Tourmaline major-element analyses were done at the Centre for Material Analysis, University of Oulu.

Sulfur isotopes were analyzed in pyrite, pyrrhotite and chalcopyrite grains from thin sections by laser ablation inductively coupled plasma mass spectrometry (LA-MC-ICP-MS). The analyses were done with a Nu Plasma HR multicollector ICP-MS together with a Photon Machine Analyte G2 laser microprobe. Analyzed samples were ablated in He gas (gas flows = 0.4 and 0.1 l/min) within a HelEx ablation cell (Müller et al., 2009), and sulfur isotope data were collected in static mode and at medium resolution (ΔM/M = 3000). The diameter of the laser beam was 40 μm using a fluence of 3.5 J/cm3 at 3 Hz frequency. The total sulfur signal obtained was typically 1.5–5 V for pyrite and 0.8–1.1 V for pyrrhotite and chalcopyrite. A 20 s baseline measurement was followed by 50–60 s of ablation for an internal precision of $^{34}S/^{32}S \leq \pm 5 \times 10^{-6}$ (1 SE). For pyrite and pyrrhotite, standard PPP-1 (Gilbert et al., 2014) and in-house standards Py1 and Py2 were used for external bracketing and quality control. For a $\delta^{34}S_{CDT}$ reference value of −0.6 ± 0.3‰ (1s) we have found an average value of −0.6 ± 0.5‰ (1s, n = 26) for the Py1 standard, whereas for a $\delta^{34}S_{CDT}$ reference value of −0.3 ± 0.3‰ (1s) we have found an average value of −0.2 ± 0.2‰ (1s, n = 26) for the Py2 standard during our analytical run. For chalcopyrite, in-house standard Cpy2 was used for the same purposes. For a $\delta^{34}S_{CDT}$ reference value of −0.7 ± 0.5‰ (1s) we have found an average value of −0.9 ± 0.3‰ (1s, n = 18) for the Cpy2 standard.

Tourmaline major-element analyses were done by means of a JEOL JXA-8530Fplus Field Emission Electron Microprobe (FE-EPMA). The analytical work was carried out with the following parameters: acceleration voltage of 15 kV, beam current of 10 nA, and 5 μm spot size. Tourmaline structural formulae were calculated with the WinTcac software (Yavuz et al., 2011) by normalizing to 15 cations. Boron isotopes in tourmaline were analyzed by using the same equipment as for the sulfur isotopes. During ablation the data were collected in static mode (^{10}B, ^{11}B) and samples were ablated using a fluence of 3.0 J/cm2, at 5 Hz pulse frequency, and with a 40 μm spot size. Typically, the total B signal obtained for tourmaline was 0.08 V. A 20 s baseline measurement was followed by 50–60 s of ablation for an internal precision of $^{11}B/^{10}B \leq \pm 0.0006$ (1 SE). Dravite standard BG1 (Hou et al., 2010) and schorl standard B4 (Tonarini et al., 2003) were used for external bracketing and quality control, with all reported ratios related to NBS SRM 951 using the 4.04362 $^{11}B/^{10}B$ value of this standard (Catanzaro et al., 1970). For a $\delta^{11}B$ reference value of −8.71 ± 0.18‰ (2s) measured by TIMS for Schorl B4, we found an average value of −9.1 ± 0.5‰ (1s, n = 17) during our analytical run. For a $\delta^{11}B$ reference value of −12.3 ± 0.18‰ (2s), measured by MC-ICP-MS, for dravite BG1 we found an average value of −12.7 ± 0.3‰ (1s, n = 10).

Monazite and xenotime grains were located in polished thin sections by means of a JEOL JSM5900LV (SEM) equipped with an energy dispersive X-ray spectrometer (EDS). Automatic scans of the thin sections were performed with the INCA feature phase detection software (Oxford Instruments Ltd). The U-Pb dating of selected monazite and xenotime grains was done by means of a Nu Plasma Attom single collector ICPMS connected to a Photon Machine Excite laser ablation system. Samples used for analytical work were ablated in He gas (gas flows = 0.4 and 0.1 l/min) within a HelEx ablation cell (Müller et al., 2009). The He aerosol was mixed with Ar (gas flow = 0.94–0.95 l/min) prior to entering the plasma, with the gas mixture being optimized daily for maximum sensitivity. The spot size was 15 μm, with a beam energy density of 2.17 J/cm^2 and at 5 Hz pulse frequency. Each measurement included a short pre-ablation followed by 20 s of He flushing, 10 s of on-mass background measurement, and 40 s of ablation with a stationary beam. A natural $^{238}U/^{235}U$ = 137.88 was used for calculation of ^{235}U from the signal at mass 238. Common ^{204}Pb was monitored at mass number 204, and the contribution of ^{204}Hg from the plasma was eliminated by on-mass background measurement prior to each analysis. In the ICP-MS system used for our analytical work, ^{204}Hg originates almost exclusively from the He supply and has been stable at 200–300 cps over several years. Age related common lead correction (Stacey and Kramers, 1975) was used in all analyses included in this study, as common lead contents were significantly above the detection limit (i.e., >60 cps of background-subtracted mass 204). Signal strengths on mass 206 were typically 2.5×10^4 to 3×10^4 depending on the uranium content and age of the monazite and xenotime. Monazite standards TS (905 ± 2 Ma; Budzyn et al., 2021) and A49 (1874 ± 3 Ma; Salli, 1983) and control samples A1326 (2630 ± 2 Ma, Hölttä et al., 2000), A276 (1915 ± 3 Ma; unpublished in-house standard), Bananeira (503 ± 2 Ma; Gonçalves et al., 2016) and Coqueiro (511 ± 3 Ma; Gonçalves et al., 2016) were used for calibration and quality control. For xenotime, calibration standard 5/RC1742 (336.2 ± 1.2 Ma; Tajcmanová et al., 2010) and control samples A1298 (1852 ± 2 Ma; Pajunen and Poutiainen, 1999) and A1244 (2616 ± 3 Ma; unpublished in-house standard) were used for the same purpose. Raw data were corrected and reduced to U-Pb isotope ratios using the GLITTER software (van Achterberg et al., 2001). Further data reduction, including common Pb corrections, was performed using in house excel spreadsheets. Plotting of the U-Pb isotopic data and age calculations were done using IsoplotR (Vermeesch, 2018). In our U-Pb isotope study we set the limit of acceptable concordance between 95 % and 105 %. Setting of this limit is arbitrary as different laboratories use different discordancy filters depending on the analytical methods, data processing techniques, and geological question of the study; the filter chosen in our study has been used in other U-Pb geochronological studies on orogenic Au deposits from the CLB (e.g., Molnár et al., 2018). When Mode I regression (Ludwig, 2012) was used to calculate upper intercept ages, the lower concordia intercept was set to 0 Ma.

4. Results

4.1. Sulfur isotopes

Examples of analyzed sulfides from Hirvilavanmaa and Naakenavaara are presented in Fig. 3. and the results of sulfur isotope analyses are shown in Fig. 4. Analytical data are presented in more detail in Supplementary Table S1. Sulfur isotope analyses were done on the sulfide grains previously measured for trace element concentrations by Vasilopoulos et al. (2023), whereby the sulfur isotope analytical spots were placed next to the craters from trace element analyses (distance <30 μm).

Sulfides from Hirvilavanmaa have a total range of $\delta^{34}S$ values between −7.2‰ and +16.5‰ with a median value of +1.2‰ (st. dev = 3.7); pyrite and chalcopyrite have median values of +1.3‰ (st. dev = 3.8) and +0.9‰ (st. dev = 1), respectively. The three pyrite populations have similar distribution of $\delta^{34}S$ values (Fig. 4b). Py_{Hirvi}-1 has a median $\delta^{34}S$ value of +0.6‰ (st. dev = 2.7), whereas Py_{Hirvi}-2, and Py_{Hirvi}-3 have medians of +1.6‰ (st. dev = 4.4) and +1.2‰ (st. dev = 3.5), respectively.

The distribution of sulfide $\delta^{34}S$ values from Naakenavaara is significantly different, having a total range between +3.1‰ and +16.2‰ with a median of +9.9‰ (st. dev = 2.4). Pyrite, chalcopyrite and pyrrhotite

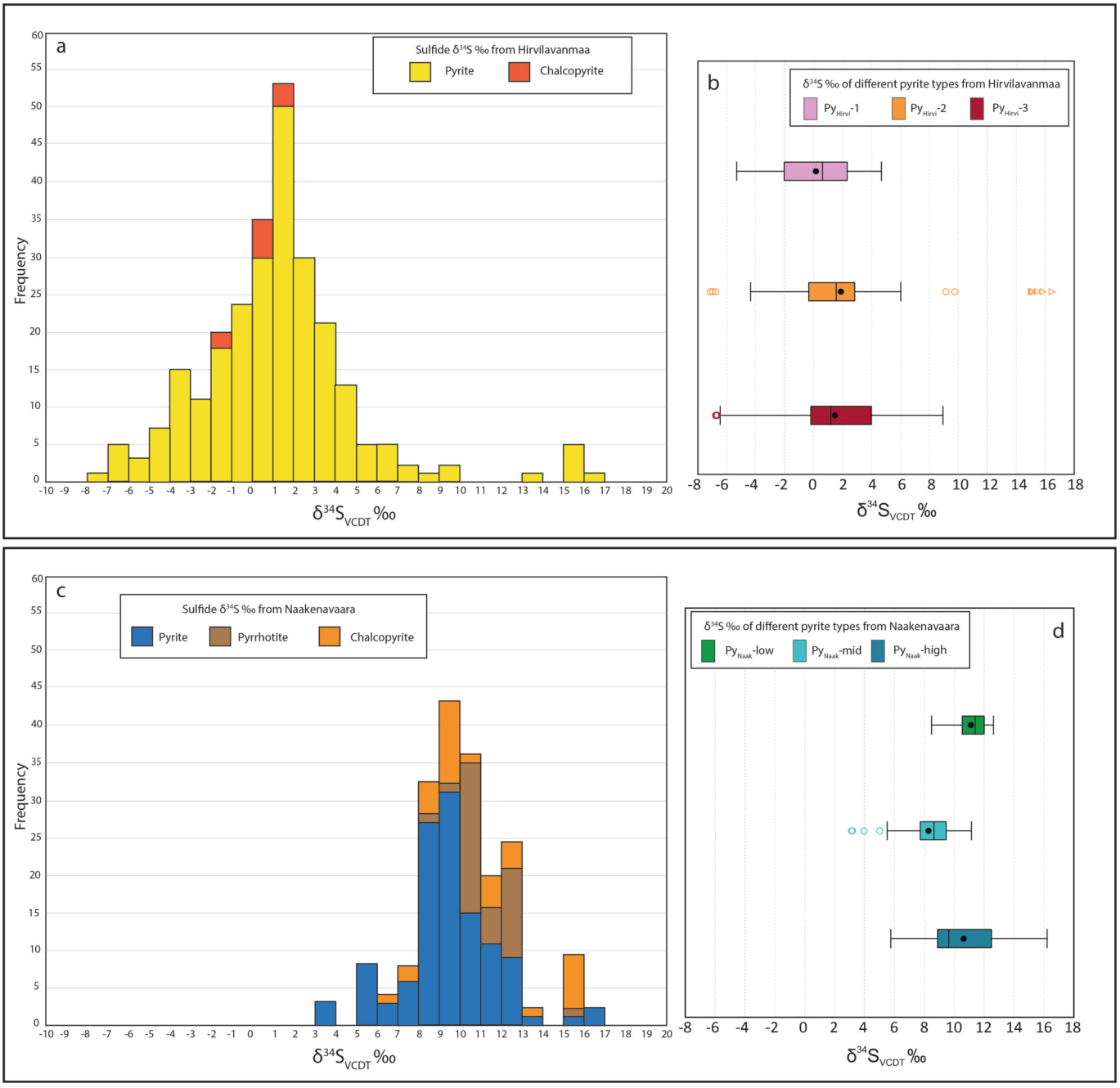

Fig. 4. (a) Histogram showing distribution of $\delta^{34}S$ values for analyzed pyrite, pyrrhotite, and chalcopyrite from Hirvilavanmaa. (b) Comparative $\delta^{34}S$ boxplots for the different pyrite generations from Hirvilavanmaa. (c) Histogram showing distribution of $\delta^{34}S$ values for analyzed pyrite, pyrrhotite, and chalcopyrite from Naakenavaara. (d) Comparative $\delta^{34}S$ boxplots for the different pyrite generations from Naakenavaara.

have median values of +9.3‰ (st. dev = 2.3), +10‰ (st. dev = 2.7), and +11‰ (st. dev = 1.3), respectively. Pyrite deposited during the late overprinting Au-rich event at Naakenavaara (Py_{Naak}-low; Vasilopoulos et al., 2023) has a median $\delta^{34}S$ of +11.2‰ (st. dev = 1.1). Pyrite deposited during the early Co- and Cu-rich stages of mineralization (Py_{Naak}-mid and Py_{Naak}-high; Vasilopoulos et al., 2023) has median $\delta^{34}S$ values of +8.6‰ (st. dev = 1.9) and +9.6‰ (st. dev = 2.5), respectively (Supplementary Table S1).

4.2. Tourmaline crystal chemistry

At Hirvilavanmaa, two tourmaline types are found mostly confined to pyrite- and chlorite-rich alteration haloes adjacent to quartz-carbonate veins (Fig. 5). Type I_H tourmaline is present in altered host rocks that still show regional pre-ore alteration assemblages including talc and early carbonate. Samples hosting Type I_H tourmaline are dominated by Py_{Hirvi}-1, indicating that they represent the early stages of Au deposition. Type I_H tourmaline is disseminated and forms clusters, typically intergrown with pyrite (Fig. 5a–c); individual grains locally exceed 200 μm in diameter. Type II_H tourmaline is present in more intensely altered parts of ore zones, in which the earliest alteration assemblages have been mostly overprinted by later albitization, carbonatization, and ore-related quartz veining and chlorite alteration. These parts of the ore zones are dominated by Py_{Hirvi}-2 and Py_{Hirvi}-3. Type II_H tourmaline is also closely associated with pyrite and typically forms clusters or locally individual disseminated grains (Fig. 5d–f); the

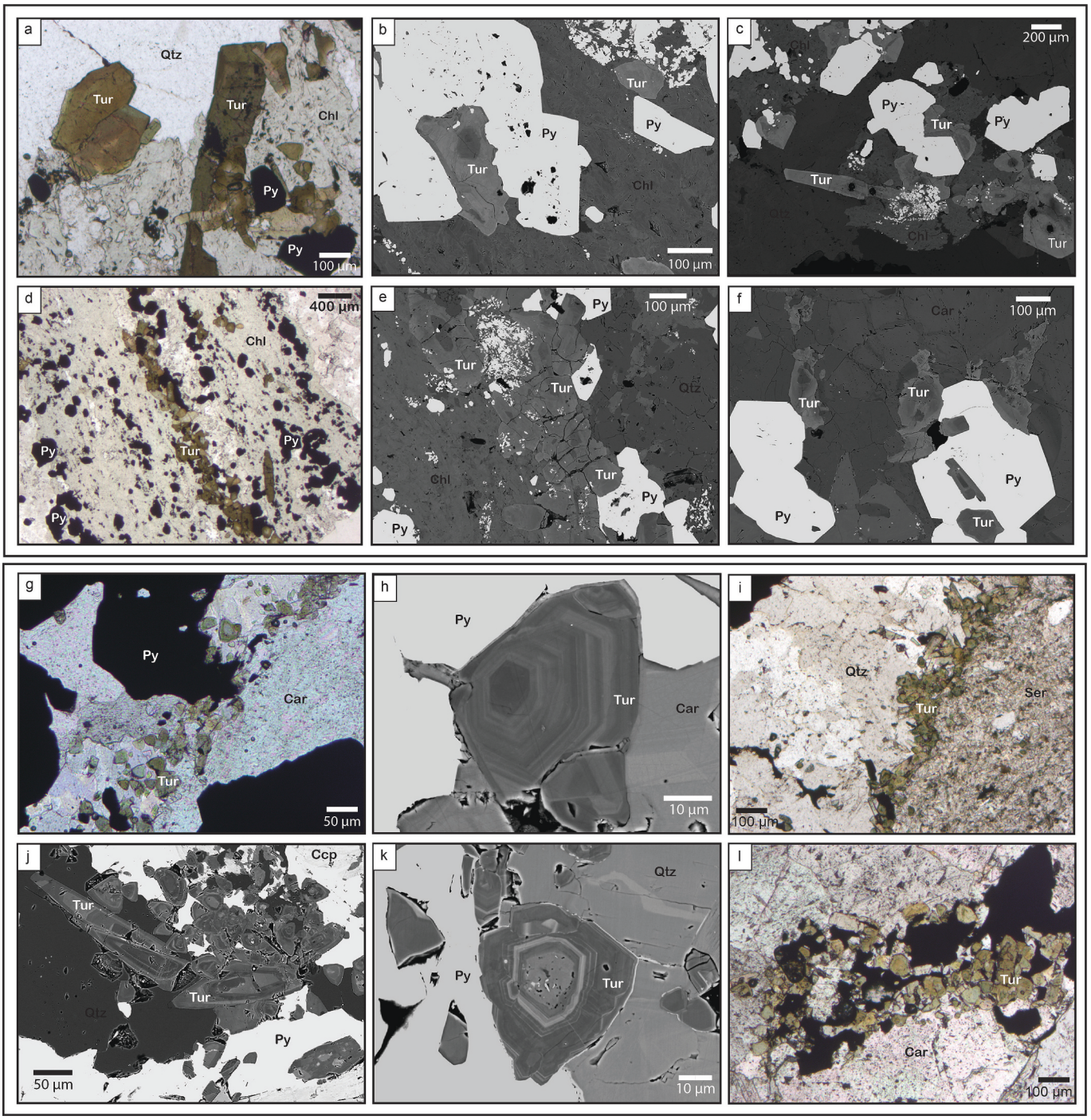

Fig. 5. (a) Photomicrograph depicting Type I_H tourmaline from Hirvilavanmaa hosted in a chlorite-rich alteration halo of a quartz-carbonate vein. (b) BSE image showing examples of analyzed Type I_H tourmaline grains from Hirvilavanmaa. (c) BSE image showing examples of analyzed Type I_H tourmaline grains from Hirvilavanmaa. (d) Photomicrograph depicting Type II_H tourmaline from Hirvilavanmaa hosted in a pyrite-hosting chlorite sheet from an ore zone. (e) BSE image showing examples of analyzed Type II_H tourmaline grains from Hirvilavanmaa. (f) BSE image showing examples of analyzed Type II_H tourmaline grains from Hirvilavanmaa closely associated with pyrite. (g) Photomicrograph depicting Type I_N tourmaline from Naakenavaara in a quartz-carbonate vein. (h) BSE image of a characteristic example of an analyzed Type I_N tourmaline grain from Naakenavaara intergrown with pyrite. (i) Photomicrograph depicting Type II_N tourmaline from Naakenavaara rimming a quartz-carbonate vein. (j) BSE image showing examples of analyzed Type II_N tourmaline grains from Naakenavaara. (k) BSE image showing a characteristic example of an analyzed Type II_N tourmaline grain from Naakenavaara. (l) Photomicrograph depicting Type II_N-b tourmaline from Naakenavaara intergrown with sulfides in a quartz-carbonate vein.

diameter of individual grains is typically <100–150 µm.

At Naakenavaara two tourmaline types were also identified (Fig. 5g–l). Type I_N is hosted by quartz-carbonate veins in altered metasedimentary host rocks in a pyrite-dominant Co-rich ore zone and forms disseminated, mostly round grains typically between 15 and 35 µm in size that are embedded in vein quartz and carbonate and locally intergrown with Py_{Naak}-mid. Tourmaline type II_N is present in ore zones characterized by Cu (±Co) enrichment that are dominated by pyrrhotite, chalcopyrite and Py_{Naak}-high. Tourmaline II_N typically forms aggregates of rounded and elongated prismatic grains (length of individual grains

~30 and 150 μm, respectively) and is typically intergrown with sulfides and biotite or forms rims to the veins. Type II_N is hosted by quartz-carbonate veins in mainly metasedimentary host rocks; Type II_N-b is a subtype of Type II_N tourmaline that is otherwise similar to Type II_N, except for being hosted by a carbonate-rich vein in altered ultramafic metavolcanic rock in a sample with low-grade Cu-Co enrichment. No tourmaline was found in samples hosting Py_{Naak}-low associated with the late Au-rich stage.

The chemical composition of the different tourmaline types from Hirvilavanmaa and Naakenavaara is presented in Supplementary Table S2. Both tourmaline types from Hirvilavanmaa have dravite compositions (Fig. 6a) with Fe/(Fe + Mg) ratios from 0.2 to 0.5 and low Al contents (mostly <6 apfu). In both Type I_H and Type II_H the contents of Ca (means of 0.01 and 0.02 apfu, respectively) and X-site vacancies (means of 0.02 and 0.10 apfu, respectively) are notably low. Na contents are generally high in both Type I_H and Type II_H, (mean values of 0.97 and 0.88 apfu, respectively). Type I_H tourmaline has particularly high Cr contents (mean of 1.10 apfu); Cr contents in Type II_H tourmaline are lower but still generally high (mean of 0.36 apfu). Mean Fe_{tot} + Mg values are 3.42 and 2.99 apfu for Type I_H and Type II_H respectively. Despite the presence of visible zoning in both tourmaline types in BSE images (Fig. 5), compositions between cores and rims generally have no differences, with mean values and standard deviations of most elements being very similar in both cases. The only exception is Cr, with concentrations being higher in the rims for both tourmaline types. On the AFM diagram, Type I_H tourmaline plots below the dravite-schorl line (Fig. 6c); Both tourmaline types align with the oxy-dravite to povondraite join. In terms of substitution vectors, $Mg(OH)(AlO)_{-1}$ appears important for Type I_H tourmaline (Fig. 7a, c, e), whereas $FeAl_{-1}$ and/or $AlO(Fe(OH))_{-1}$ exchange vectors seem stronger for Type II_H tourmaline, with the data plotting subparallel to the respective vectors in Fig. 7. Slight displacements from the vectors indicate the effect of other substitutions such as $Mg(OH)(AlO)_{-1}$.

Most tourmaline from Naakenavaara has a dravite composition, except for roughly a third of Type II_N that plot in the schorl quadrant of Fig. 6b. Both tourmaline types are characterized by moderate Al contents (mean values close to 6 apfu). Mean Na values are ~0.80 apfu for all types. Contents of Cr are high in Type II_N-b (mean 0.44 apfu) and significantly lower in Types I_N and II_N (means of 0.02 and 0.01 apfu respectively). Fe_{tot} + Mg values are generally <3 apfu for all tourmaline types. For all tourmaline types in Naakenavaara there is not any notable variation in major element composition between cores and rims. On the AFM diagram, most tourmaline data plot above the schorl-dravite line (Fig. 6d). Type I_N tourmaline mostly aligns with the oxy-dravite to povondraite trend (Fig. 6d). All tourmaline types from Naakenavaara show signs of the effect of different substitutions (Fig. 7b, d, f). The $MgFe_{-1}$ substitution seems to affect all tourmaline types (Fig. 7b). The other most significant substitutions appear to be, $FeAl_{-1}$ and/or $AlO(Fe(OH))_{-1}$ for tourmaline types I_N and II_N (Fig. 7d, f), and $Mg(OH)(AlO)_{-1}$ for Type II_N-b (Fig. 7f).

4.3. Tourmaline boron isotopes

Results of in situ boron isotope analyzes of tourmaline from Hirvilavanmaa and Naakenavaara are shown in Fig. 8 and in detail on Supplementary Table S3. At Hirvilavanmaa, Type I_H tourmaline has $\delta^{11}B$ values ranging between −8.2 and −3.2‰ and a mean of −5.6‰; cores and rims from this population have similar mean $\delta^{11}B$ values of −5.8‰ and −5.4‰ respectively. Type II_H tourmaline has $\delta^{11}B$ values ranging between −9.6 and −5.5‰ and a mean of −8.2‰; in this tourmaline

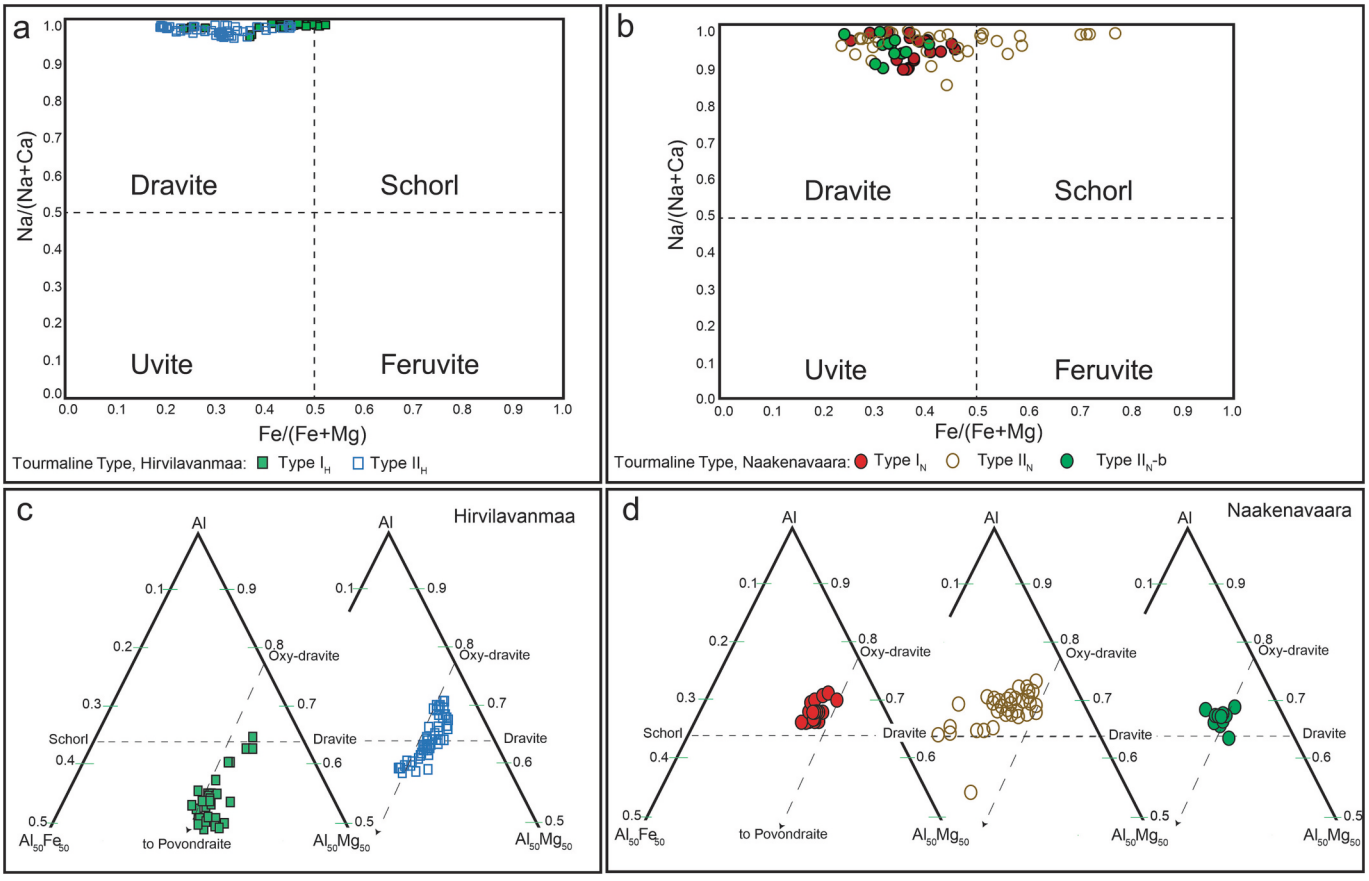

Fig. 6. (a–b) Classification of tourmaline types from (a) Hirvilavanmaa and (b) Naakenavaara based on Fe/(Fe + Mg) vs. Na/(Na + Ca) plots. Modified after Jiang et al. (2002); (c–d) Al–Fe–Mg ternary plot after Henry and Guidotti (1985) depicting tourmaline types from (c) Hirvilavanmaa (d) and Naakenavaara.

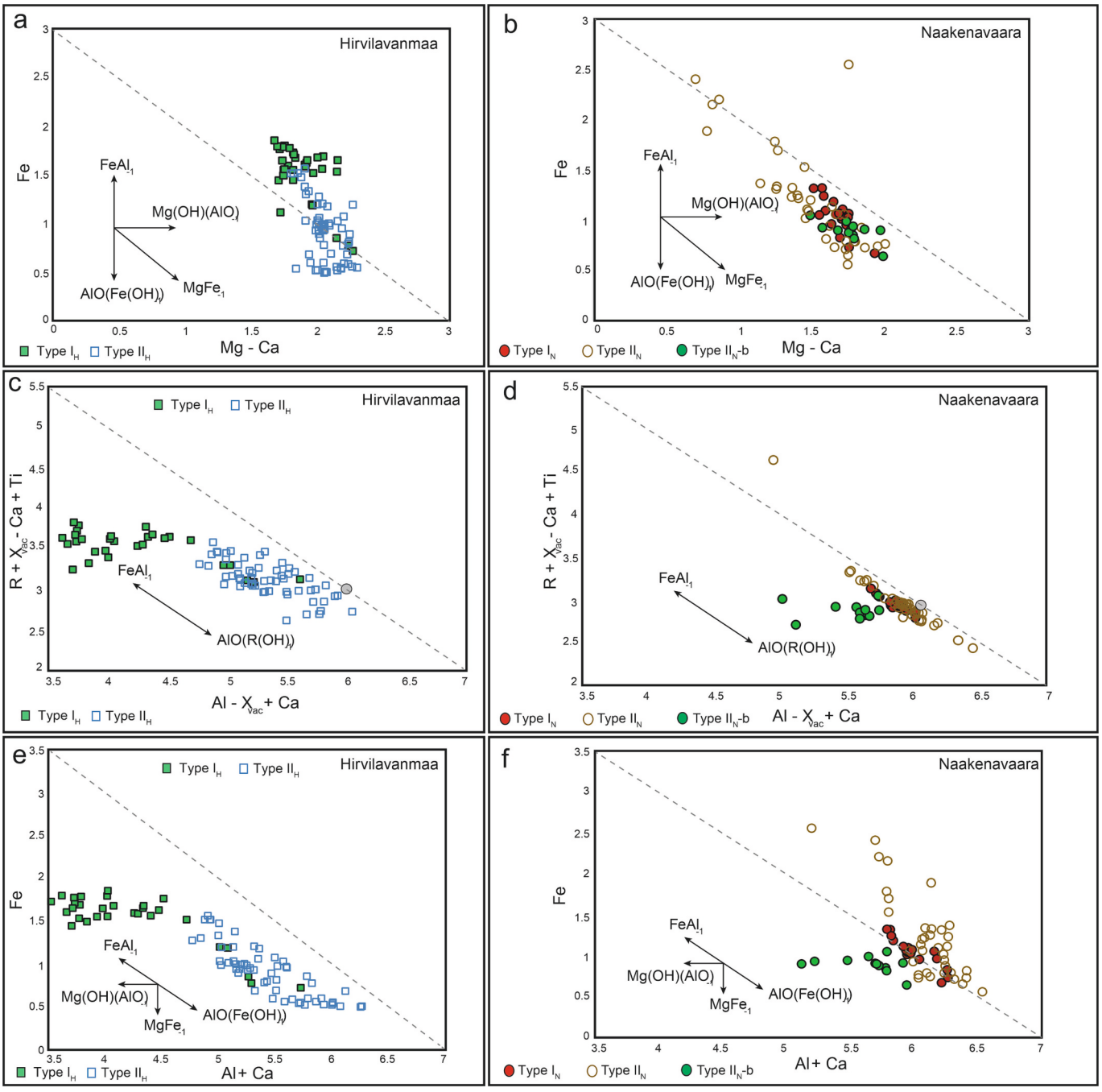

Fig. 7. (a–b) Mg-Ca vs. Fe binary for tourmaline types from (a) Hirvilavanmaa and (b) Naakenavaara after Henry et al. (2008), The Mg-Ca value represents a projection down the $CaMg(NaAl)_{-1}$ exchange vector and it accounts for the influence of Ca on the overall Mg content; (c–d) Al-X-site vacancy + Ca vs. R + X-site vacancy-Ca + Ti binary for tourmaline from (c) Hirvilavanmaa and (d) Naakenavaara (after Henry et al., 2008). The parameters used on the axes are derived from projecting down the $MgFe_{-1}$, $X_{vac}Al(NaR)_{-1}$, $CaMg(NaAl)_{-1}$, and $TiO_2(R(OH)_2)_{-1}$ exchange vectors. R represents the sum of Mg + Fe, corresponding to the projection down the MgFe-1 exchange vector. Dravite and schorl are projected to the same point in this diagram, and the influence of the $FeAl_{-1}$ and $Alo(R(OH))_{-1}$ exchange can be isolated; (e–f) Al + Ca vs. Fe binary for tourmaline types from (e) Hirvilavanmaa and (f) Naakenavaara (after Henry et al., 2008). The value of Al + Ca represents a projection down the $CaMg(NaAl)_{-1}$ exchange vector and it accounts for the influence of Ca on the overall Al content.

population, cores and rims have a mean $\delta^{11}B$ value of −8.7‰ and −7.7‰ respectively.

At Naakenavaara, tourmaline Types I_N and II_N-b were analyzed. Tourmaline from these samples has $\delta^{11}B$ values ranging between −10.6 and −7.7‰ and a mean of −9.4‰. No core and rim distinctions were made for analyzed tourmaline from Naakenavaara due to the small grain size.

4.4. U-Pb dating of monazite and xenotime

In both studied deposits most of the detected monazite and xenotime grains were in the altered host rocks and small, typically <40 μm in length. Especially at Hirvilavanmaa a significant proportion of the detected grains had a length of ~12–20 μm. In both deposits these small grains were anhedral and full of tiny inclusions. We attempted U-Pb age dating on this type of grains in both deposits, but the results were either strongly discordant or heavily scattered and had in many cases

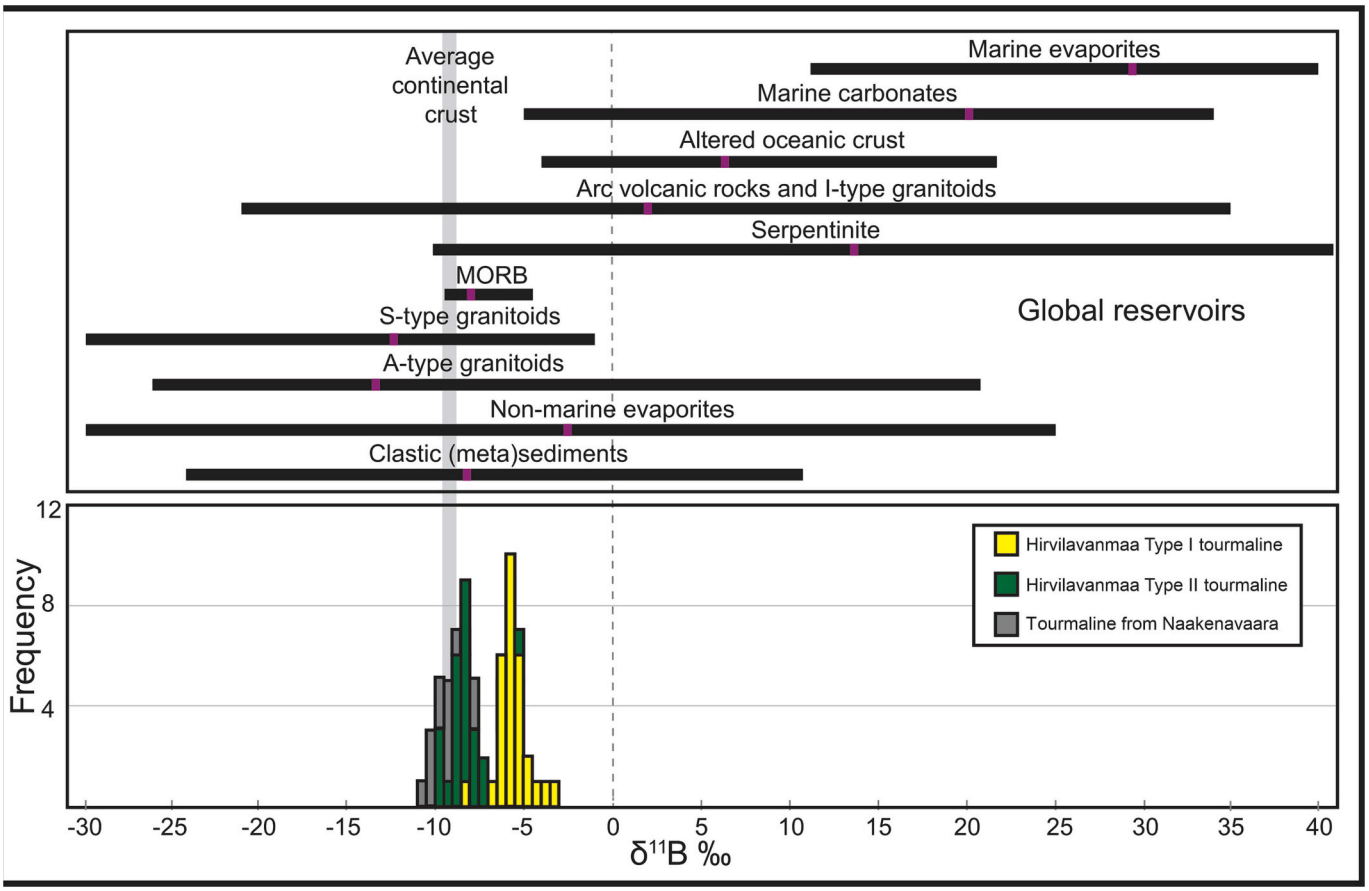

Fig. 8. (a) Histogram showing distribution of $\delta^{11}B$ values for analyzed tourmaline from Hivrilavanmaa and Naakenavaara and a comparison with global boron reservoirs; reservoir data modified after Trumbull et al. (2020). Purple rectangles inside the reservoir ranges are median values based on the data compilation from Trumbull et al. (2020). (For interpretation of the references to colour in this figure legend, the reader is referred to the web version of this article.)

particularly large common Pb values and errors; thus, results from these grains are unreliable and we do not consider them for further evaluation. Xenotime and monazite grains big enough for reliable concordant results were found in sulfide-hosting veins at Naakenavaara and in sulfide-rich chlorite alteration haloes adjacent to veins in host rocks at Hirvilavanmaa, and results from these grains are presented below.

At Naakenavaara, two relatively large (160 and 175 μm in length) xenotime grains were found in a cobalt- and copper-rich ore zone intergrown with pyrrhotite in quartz-carbonate veins (Fig. 9a–b); these veins host pyrite that is associated with the main Cu-rich stage of the first base metal-rich mineralizing event (Py_{Naak}-high). This type of xenotime (NK-xnt-1; NK stands for Naakenavaara) is subhedral to euhedral and relatively free of inclusions. Multiple analytical spots were placed on these grains, most of them providing concordant results (Supplementary Table S4). The concordia age for these spots (n = 16) is 1804 ± 3.3 Ma (MSWD = 0.5; Fig. 10a) and the weighted mean $^{207}Pb/^{206}Pb$ age is 1802.3 ± 3.5 Ma (MSWD = 3.5; Fig. 10b). Smaller (up to 50 μm in length), inclusion-free, mostly subhedral xenotime (NK-xnt-2) was found in a quartz-carbonate vein from another sample belonging to a Co-only ore zone; all analyzed xenotime grains are situated close to pyrite (Py_{Naak}-mid) or intergrown with it (Fig. 9c–e). Half of the analytical spots in these xenotimes provided concordant results (n = 3). An upper intercept age of 1816 ± 10 Ma (MSWD = 0.68; Fig. 11c) was calculated using Mode I regression (Ludwig, 2012). Several monazite grains were found in late carbonate-quartz veins that are associated with the late Au-rich overprinting event (Vasilopoulos et al., 2023). This type of monazite (NK-mnz-1) is mostly round, ~30 to 70 μm in size, and free of inclusions; it appears either intergrown with sulfides or close to them embedded in vein quartz and carbonate (Fig. 9f–i). Most analytical spots (n = 15) provided concordant, yet variable results and an upper intercept age of 1752 ± 10 Ma (MSWD = 0.59) was calculated (Fig. 11d).

At Hirvilavanmaa, a few small xenotime and monazite grains were found in chlorite (±tourmaline)-rich parts of ore zones that also host pyrite and are adjacent to quartz-carbonate veins. This type of xenotime (Hirvi-xnt-1; Hirvi stands for Hirvilavanmaa) is subhedral, approximately 25 μm in length, and relatively free of inclusions (Fig. 10a–c). Three analytical spots gave concordant results and an upper intercept age of 1822 ± 9 Ma (MSWD = 0.96) was calculated (Fig. 12a). Monazite grains (Hirvi-mnz-1) found in the chlorite-rich parts of ore zones were also relatively free of inclusions and ~20–30 μm in length (Fig. 10d–f). Most of these monazite grains provided concordant results (n = 4) and an upper intercept age of 1785 ± 10 Ma (MSWD = 1.3) was calculated (Fig. 12b).

5. Discussion

5.1. Interpretation of U-Pb age data and implications for metallogeny of orogenic Au deposits in the CLB

Previous studies have found that monazite can be subject to alteration that disturbs its U-Pb system even under moderately high temperature fluids (Seydoux-Guillaume et al., 2012; Williams et al., 2001); xenotime can also undergo alteration, especially under acidic conditions (Hetherington and Harlov, 2008; Hetherington et al., 2010), something that was proposed for xenotime from the Iso-Kuotko deposit in the CLB (Molnár et al., 2018). Most of the detected xenotime and monazite grains in both deposits studied here were embedded in altered host rocks

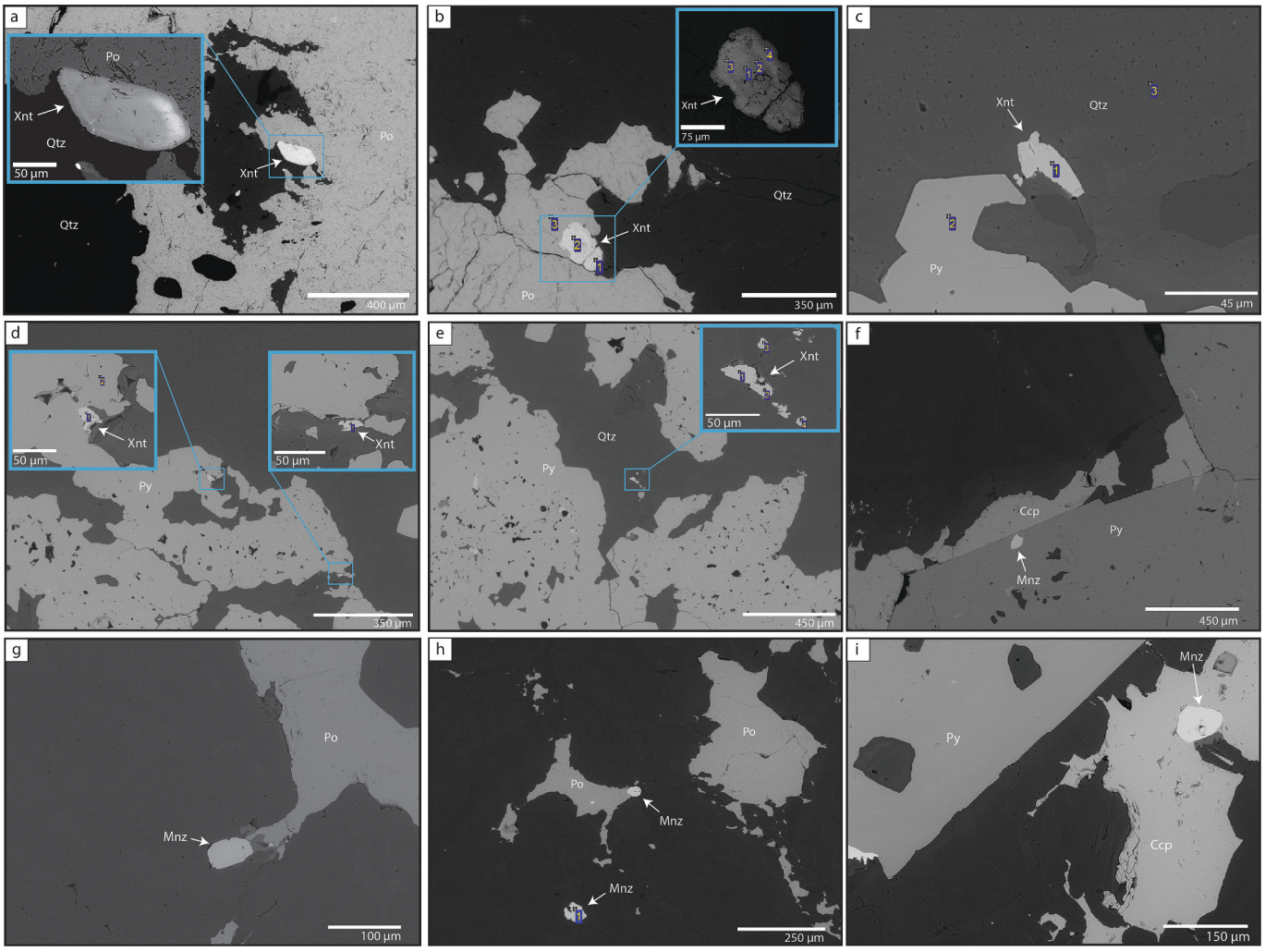

Fig. 9. BSE images showing characteristic examples of analyzed xenotime and monazite from Naakenavaara. Numbered spots in some grains depict sites of spectral EDS analysis with the SEM. (a) Large, euhedral xenotime (NK-xnt-1) grain intergrown with pyrrhotite. Inset image shows a close-up of the same grain. (b) Large xenotime (NK-xnt-1) grain intergrown with pyrrhotite. Inset image shows a close-up of the same grain with higher contrast. (c) Xenotime (NK-xnt-2) in a quartz-carbonate vein. (d) Xenotime grains (NK-xnt-2) intergrown with pyrite. Inset images show close-ups of the xenotime grains. (e) Xenotime (NK-xnt-2) in a quartz-carbonate vein close to pyrite. Inset image shows a close-up of the xenotime. (f) Monazite (NK-mnz-1) as an inclusion in pyrite (g) Monazite (NK-mnz-1) in a quartz-carbonate vein adjacent to patchy pyrrhotite (h) Monazite (NK-mnz-1) grains intergrown with pyrrhotite and embedded in vein quartz (i) Monazite (NK-mnz-1) as an inclusion in chalcopyrite within a quartz-carbonate vein.

and gave problematic analytical results that were largely discordant. As previously described, this was partially due to the small size of the analyzed grains that were marginally larger in length (ca. 12–20 µm) compared to the diameter of the laser beam (15 µm), but we propose that the altered nature of these grains and the presence of inclusions also played a role and prevented calculations of precise U-Pb ages.

At Naakenavaara, the U-Pb system in xenotime from quartz-carbonate veins in Co- and Cu-rich ore zones appears to be undisturbed based on the large proportion of concordant data (Supplementary Table S4). The ore zones that host this type of xenotime formed during the main base metal-rich mineralizing event as established by Vasilopoulos et al. (2023). Concordant xenotime hosted in a quartz-carbonate vein that also hosts abundant pyrite (Py_{Naak}-mid; Vasilopoulos et al., 2023) in a Co-only ore zone provided an upper intercept age of 1816 ± 10 Ma. This age is considered as representing the early Co-rich stage of the base metal-rich mineralizing event at Naakenavaara and it essentially marks the beginning of ore deposition in the deposit. The 1804 ± 3.3 Ma concordia age of xenotime inclusions in pyrrhotite within quartz-carbonate veins that host pyrite (Py_{Naak}-high) associated with the Cu-rich stage of mineralization is considered as the age for the main Cu-rich stage in the deposit. These ages correspond to a regional deformation event at 1.82–1.80 Ga, which relates to an oblique collision of the Volgo-Sarmatia and Fennoscandia protocontinents (Bogdanova et al., 2015; Sayab et al., 2021) and corresponds to the D4 deformation stage in the CLB as established by Sayab et al. (2020). Based on these ages and considering the relative timing of mineralizing events established by Vasilopoulos et al. (2023), base metal-rich mineralization at Naakenavaara began by Co deposition during the beginning of the 1.82–1.80 Ga D4 deformation and had transitioned to the main Cu-rich phase by its waning stages. At Hirvilavanmaa, two xenotime grains in a pyrite-hosting chlorite-rich alteration halo of a quartz-carbonate vein give an upper intercept age of 1822 ± 9 Ma. Based on this, we propose that vein opening and pyrite deposition started at Hirvilavanmaa during the same time as the base metal mineralization at Naakenavaara. Molnár et al. (2019) recorded ~1820 Ma ages from monazite hosted in the major carbonate-sulfide veins of the Saattopora deposit, showing that this deformation event was important for ore deposition of both base metal-rich and Au-only deposits along the SiSZ. The same event caused re-opening of previously formed veins in the Iso-Kuotko deposit in the KiSZ without gold mineralization (Molnár et al., 2018), showing that

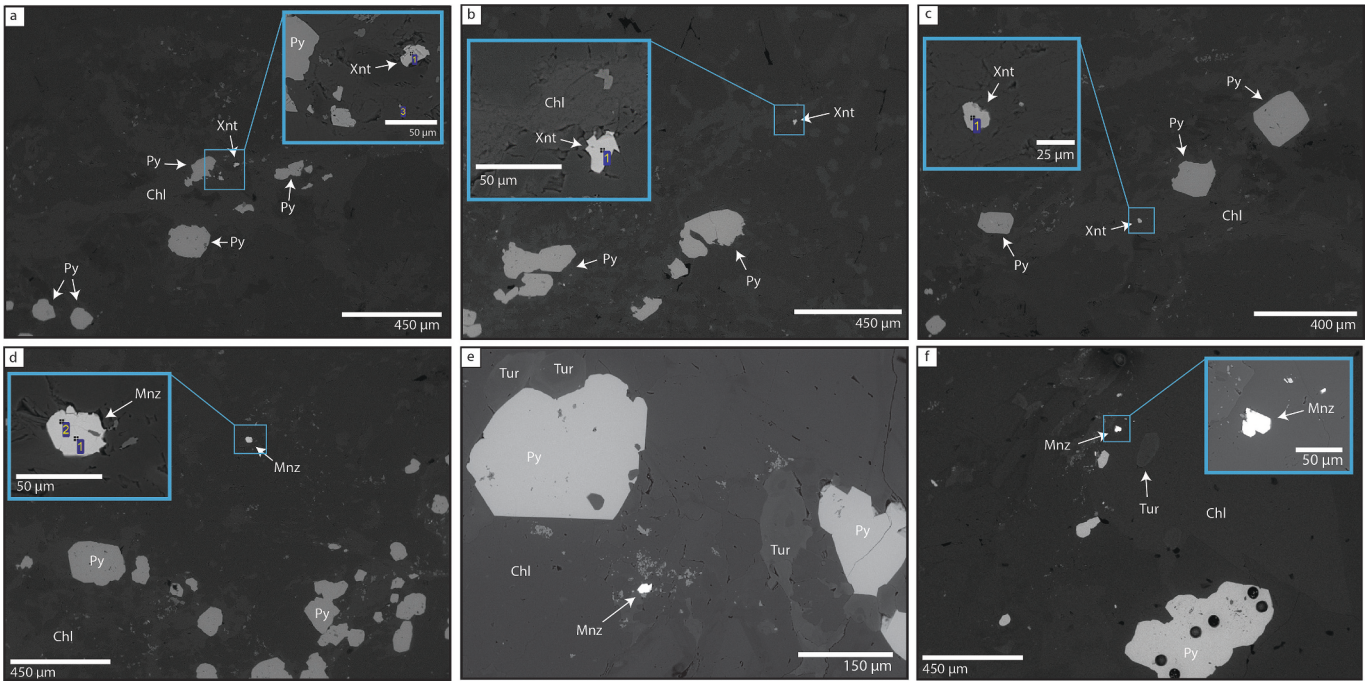

Fig. 10. BSE images showing characteristic examples of analyzed xenotime and monazite from chlorite-rich alteration haloes of quartz-carbonate veins from Hirvilavanmaa. Numbered spots in some grains depict sites of spectral EDS analysis with the SEM. (a) Analyzed xenotime grain (Hirvi-xnt-1) close to disseminated pyrite. Inset image shows a close-up of the xenotime grain. (b) Analyzed xenotime grain (Hirvi-xnt-1). Inset image shows a close-up of the xenotime. (c) Analyzed xenotime grain (Hirvi-xnt-1) close to disseminated pyrite. Inset image shows a close-up of the xenotime. (d) Analyzed monazite (Hirvi-mnz-1) grain hosted in the same chlorite sheet that hosts several disseminated pyrite grains. Inset image shows a close-up of the monazite. (e) Analyzed monazite grain (Hirvi-mnz-1) close to tourmaline and pyrite. (f) Analyzed monazite grain (Hirvi-mnz-1) close to disseminated pyrite and tourmaline. The circular pits in the big pyrite grain are from sulfur isotope and trace element LA-ICP-MS analytical work. Inset image shows a close-up of the monazite.

during this deformation event the conditions for ore formation were probably less ideal in the KiSZ compared to the SiSZ.

Hydrothermal monazite from late carbonate veins that host pyrite (Py_{Naak}-low) associated with the Au mineralization at Naakenavaara provided mostly concordant results. The 1752 ± 10 Ma age from these monazites corresponds within error to the late waning stages of the Svecofennian orogeny and to the D5 deformation in the CLB as established by Sayab et al. (2020) and related to E-W shortening at ca. 1.77–1.76 Ga. At Hirvilavanmaa, monazite from pyrite-hosting alteration haloes of quartz-carbonate veins in ore zones give an age of 1785 ± 10 Ma, which we consider as representing the main Au-depositing stage at Hirvilavanmaa. This age could fit within error either with an orogenic extension stage at ca. 1.80–1.77 Ga before the final deformation stage (D5; Sayab et al., 2020), or with the late 1.77–1.76 deformation stage that affected Au deposition at Naakenavaara. Similar ages of mineralizing events corresponding to the late (post 1.80 Ga) deformation stages in the CLB have been established in the Saattopora (Mänttäri, 1995; Molnár et al., 2017) and Levijärvi-Loukinen (Molnár et al., 2017) deposits along the SiSZ and the Iso-Kuotko deposit along the KiSZ (Molnár et al., 2018), proving that these late stages of deformation were metallogenically important for deposits along both the SiSZ and the KiSZ, the two most significant structures in the CLB.

Vasilopoulos et al. (2023) suggested based on mineralogical, lithogeochemical and sulfide trace element characteristics, that base metal mineralization started with Co deposition and developed into the main Cu-rich stage, and that Au deposition was a separate late overprinting event at Naakenavaara. Additionally, Hulkki and Keinänen (2007) concluded that Au mineralization in the Hirvilavanmaa deposit took place late in the structural history of the CLB, postdating peak metamorphic conditions. Results from our U-Pb geochronological study on hydrothermal xenotime and monazite confirm these observations.

5.2. Tourmaline crystal chemistry

The chemical composition of tourmaline can reflect fluid chemistry, formation conditions and composition of the host rocks (e.g., Henry and Dutrow, 1996; Henry et al., 2008; Hazarika et al., 2015; Sciuba et al., 2021). In systems with high fluid/rock ratios the major element composition of tourmaline is buffered by the fluid phase and the influence of host rock composition is comparatively small (Slack and Coad, 1989). At Hirvilavanmaa, both tourmaline types that are hosted by altered ultramafic metavolcanic host rocks have abnormally high Cr contents (mean Cr_2O_3 of 7.7 and 2.6 wt% for Types I_H and II_H, respectively) compared to the typical concentrations in tourmaline from orogenic gold deposits (Cr_2O_3 ~0.2 wt%; Sciuba et al., 2021). Similarly, Type II_N-b tourmaline from Naakenavaara is hosted by ultramafic metavolcanic rocks and also has elevated Cr contents (mean Cr_2O_3 of 2.5 wt %). Tourmaline types I_N and II_N, on the other hand, are hosted in metasedimentary rocks and have much lower Cr contents (mean Cr_2O_3 of 0.14 and 0.08 wt%, respectively). This correlation of host rock type with Cr contents in tourmaline indicates a relatively strong effect of host rock composition in controlling the major element composition of tourmaline in both deposits. Additionally, pre-mineralization albitization of host rocks characterizes both Hirvilavanmaa and Naakenavaara, with the degree and extent of albitization being especially pronounced in the former deposit. The high Na contents (means mostly >0.8 apfu) in all tourmaline types from the two deposits supports for a relatively strong lithological control on tourmaline composition. Finally, whereas the Mg $(OH)(AlO)_{-1}$ exchange seems to influence tourmaline types hosted by ultramafic metavolcanic rocks in both deposits (especially Type II_N-b tourmaline from Naakenavaara, and Type I_H tourmaline from Hirvilavanmaa; Fig. 7) it exerts no influence on Type I_N and II_N hosted by metasedimentary rocks. Based on the above observations, we conclude that the major element composition of tourmaline from both deposits was clearly affected by the host rock composition, which points to

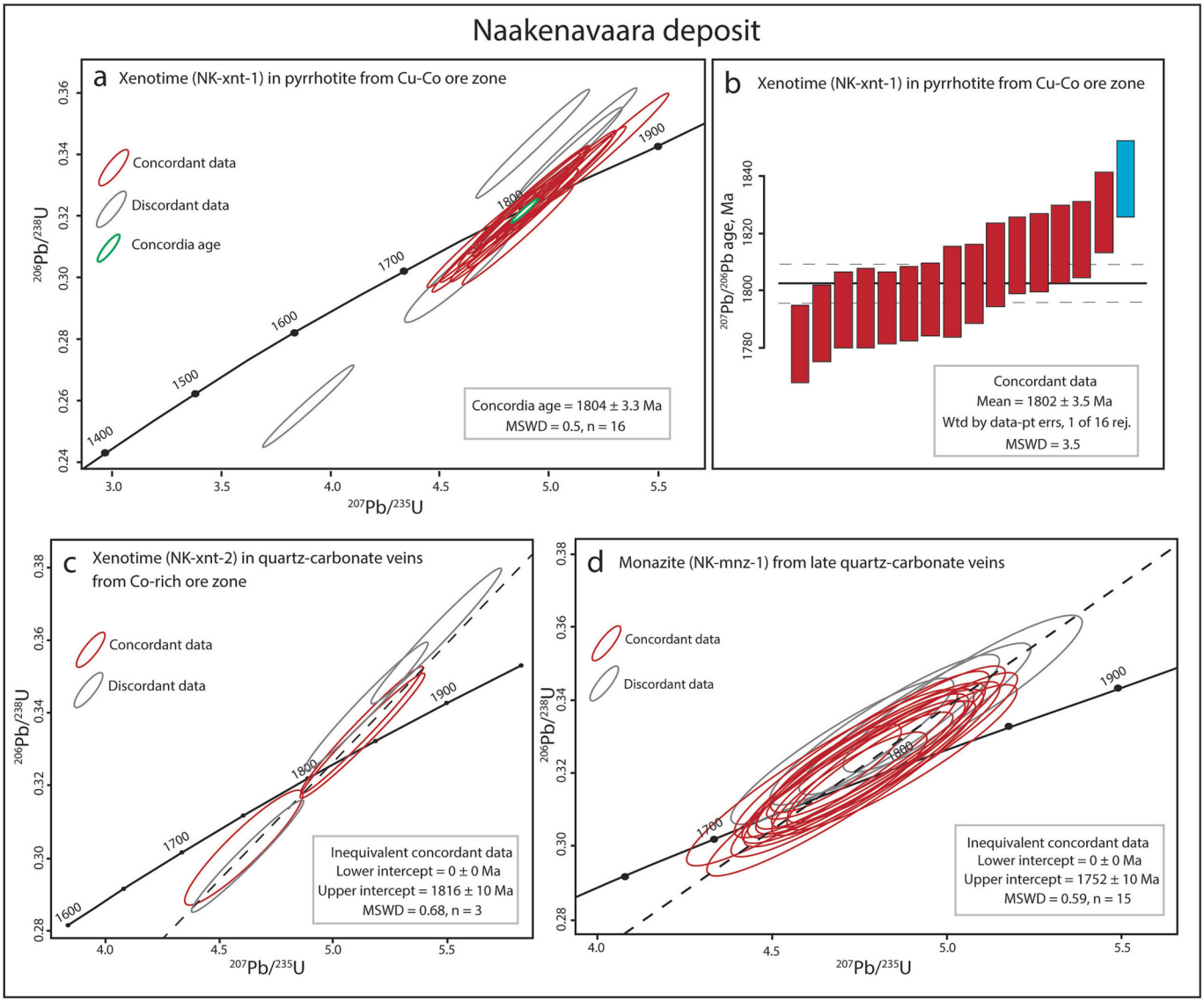

Fig. 11. (a) U-Pb concordia diagram for xenotime (NK-xnt-1) intergrown with pyrrhotite in a quartz-carbonate vein from Cu-Co ore zone at Naakenavaara. (b) Individual $^{207}Pb/^{206}Pb$ concordant data used in calculation of a weighted mean age for NK-xnt-1 xenotime. (c) U-Pb concordia diagram for xenotime (NK-xnt-2) found in quartz-carbonate veins from Co-rich ore zones at Naakenavaara. (d) U-Pb concordia diagram for monazite (NK-mnz-1) found in late quartz-carbonate veins.

relatively low fluid/rock ratios during tourmaline deposition. Type I_H tourmaline from Hirvilavanmaa has notably higher Cr and Na concentrations compared to Type II_H and shows a stronger influence of the Mg(OH)$(AlO)_{-1}$ exchange. These variations could either reflect local differences in host rock composition, different fluid chemistry or changing fluid/rock ratios. Considering that the chemistry of hydrothermal fluids involved in the different mineralizing stages at Hirvilavanmaa did not change significantly based on the trace element characteristics of pyrite (Vasilopoulos et al., 2023), changes in fluid chemistry can be excluded as the cause of this variation. Additionally, both tourmaline types are hosted by altered ultramafic metavolcanic rocks, and whereas local changes in host rock composition could have played some role, they are not enough to explain these differences. Instead, this variation in tourmaline composition could be best explained by a changing fluid/rock ratio during different mineralizing stages. A particularly low fluid/rock ratio during early mineralizing stages at Hirvilavanmaa resulted in a strong lithological control on tourmaline composition; higher (but still generally low) fluid/rock ratios in later stages of mineralization led to a comparatively weaker lithological control on the major element composition of tourmaline.

Type I_H and II_H tourmaline from Hirvilavanmaa have low Al (<6 apfu) and high Fe_{tot} + Mg values (mostly >3 apfu), implying relatively low amounts of Al in the Y-site and the presence of Fe^{3+}. There is additional evidence of Al substitution by Fe^{3+}, as both tourmaline types align close to the oxydravite to povondraite trend on an AFM diagram (Fig. 6c) and especially type II_H shows evidence of the $FeAl_{-1}$ exchange (Fig. 7a, c, e), something that also translates to an inverse correlation between Fe and Al (R^2 = 0.71). Type I_H shows some influence by the $FeAl_{-1}$ exchange, but is also strongly affected by the Mg(OH)$(AlO)_{-1}$ exchange as discussed previously. All these characteristics indicate that tourmaline at Hirvilavanmaa was deposited from a relatively oxidized fluid (e.g., Henry et al., 2008; Henry and Dutrow, 2012; Hazarika et al., 2015), which is further supported by the fact that pyrite almost exclusively dominates the sulfide mineralogy of the deposit and is accompanied locally by abundant hematite. At Naakenavaara, tourmaline types I_N and II_N are hosted by metasedimentary rocks in Co and Cu (±Co) ore zones respectively. Type I_N tourmaline has low Al (mean < 6 apfu) concentrations, mostly aligns with the oxy-dravite to povondraite join (Fig. 6d) and shows evidence of the $FeAl_{-1}$ exchange (Fig. 7d & f), suggesting a relatively high Fe^{3+}/Fe^{2+} ratio. These characteristics imply

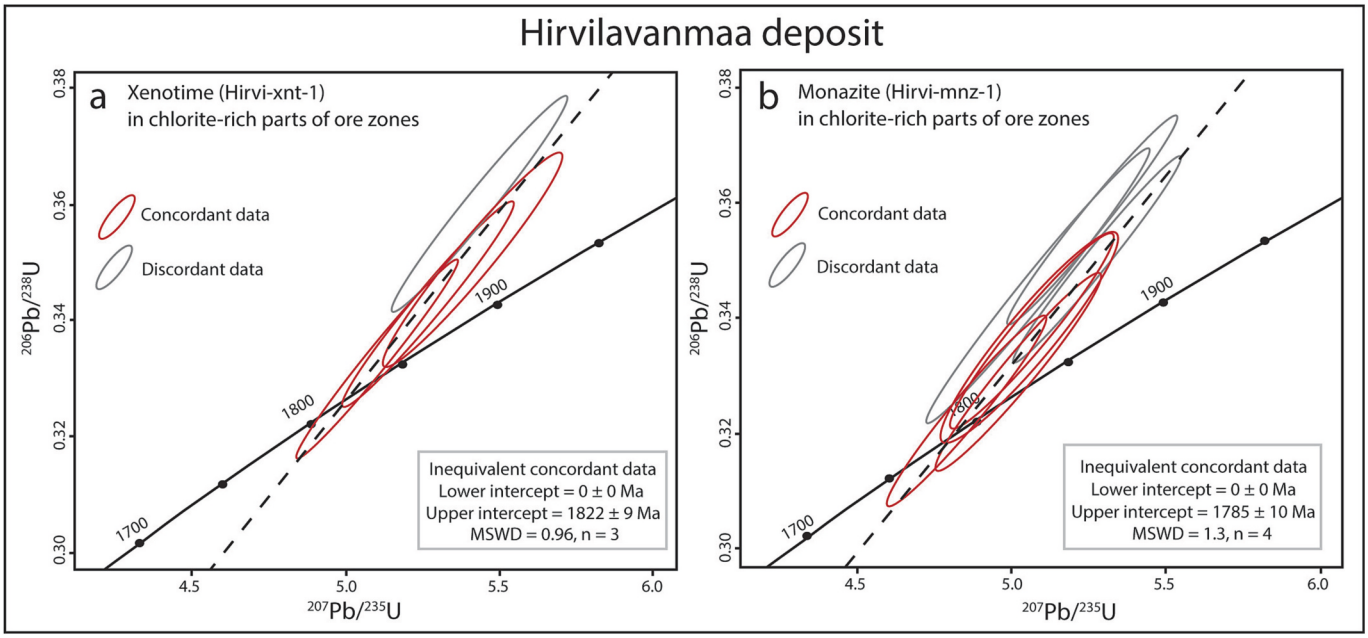

Fig. 12. (a) U-Pb concordia diagram for xenotime (Hirvi-xnt-1) found in chlorite-rich alteration haloes of quartz-carbonate veins at Hirvilavanmaa. (b) U-Pb concordia diagram for monazite (Hirvi-mnz-1) found in chlorite-rich parts of ore zones at Hirvilavanmaa.

that the hydrothermal fluid involved in the early Co-rich stage was relatively oxidized, supported by the dominance of pyrite instead of pyrrhotite during this mineralizing stage (Vasilopoulos et al., 2023). Type II_N tourmaline has higher Al (mean > 6 apfu) compared to Type I_N, and does not align with the oxydravite to povondraite trend on an AFM diagram (Fig. 6d). Type II_N shows less influence of the $FeAl_{-1}$ exchange compared to Type I_N, with other exchange vectors such as $MgFe_{-1}$, $AlO(R(OH))_{-1}$, and $AlO(Fe(OH))_{-1}$ exerting an influence (Fig. 7b, d & f). Type II_N-b hosted by ultramafic metavolcanic rocks is even less affected by the $FeAl_{-1}$ exchange. Based on the above observations we infer that during the main Cu-rich mineralizing stage the hydrothermal system was relatively reduced compared to the early Co-rich stage, which is supported by the prevalence of pyrrhotite together with chalcopyrite and the comparatively minor presence of pyrite in Cu-rich ore zones.

5.3. Constraints from boron and sulfur isotope geochemistry

Sulfur isotope ratios of sulfides from Hirvilavanmaa and Naakenavaara differ significantly, with median $\delta^{34}S$ values of +1.2‰ and +9.9‰, respectively. Several factors, such as temperature, different sources of sulfur, and redox conditions can affect the sulfur isotope composition of sulfides (e.g., Ohmoto, 1972, 1986; Hutchison et al., 2020). Based on the Se content of pyrite and the Cd/Zn ratio of chalcopyrite it has been inferred that temperature of ore formation was generally higher in Hirvilavanmaa than Naakenavaara (Vasilopoulos et al., 2023) in all mineralizing stages. However, considering that ore formation in both deposits took place late during the deformational history of the CLB in post-peak metamorphic conditions and that ore zones are hosted by greenschist facies metamorphic grade rocks, inferred differences (approximately 100 °C calculated on the basis of average Se content in pyrite; cf. Keith et al., 2018) in temperature would only cause small changes to the equilibrium isotopic fractionation factor of pyrite relative to H_2S (cf. Ohmoto and Rye, 1979; Seal, 2006), which are not enough to justify the contrasting $\delta^{34}S$ signatures in the deposits. The inferred relatively oxidizing conditions in the pyrite-dominant Hirvilavanmaa deposit as opposed to the generally more reduced conditions at Naakenavaara, could have played a role in the $\delta^{34}S$ distribution in the deposits. However, as discussed previously, crystal chemistry of tourmaline suggests that relatively oxidizing conditions prevailed during the early pyrite-dominant Co-rich stage at Naakenavaara, and Py_{Naak}-mid deposited during this stage has a significantly higher median $\delta^{34}S$ (+8.6‰) compared to pyrite from Hirvilavanmaa (+1.3‰). Thus, even if redox conditions had some effect on the sulfur isotope values of sulfides, the contrast between the deposits is most likely due to distinct sources of sulfur, especially considering that the two deposits also have distinct lithogeochemical and pyrite trace element characteristics that point towards different sources of ore-forming components (Vasilopoulos et al., 2023). Boron isotopes are a sensitive indicator for the origin of boron and fluids in various geological settings (e.g., Palmer and Swihart, 1996). The main factors controlling the boron isotope composition of tourmaline include the source rock composition, formation temperature, fluid/rock ratios, and P/T conditions of regional metamorphism (Henry and Dutrow, 1996; Jiang et al., 2002; Trumbull et al., 2020). By considering the same constraints mentioned previously for the sulfur isotope data, formation temperature and regional P/T conditions can be excluded from being the main factors controlling the observed differences in B isotope compositions between Hirvilavanmaa and Naakenavaara. Since the sulfur isotopes in the deposits seem to reflect the source of sulfur, and since fluid/rock ratios remained relatively low in both deposits based on tourmaline major element data, it is most likely that the boron isotope composition of tourmaline in the deposits is mostly a reflection of the boron source. The isotopic composition of several boron reservoirs considerably overlaps, and this can cause limitations in the identification of the boron source (Trumbull et al., 2020). In our study, we interpret tourmaline boron isotopes in combination with sulfur isotopes to reduce uncertainties from overlapping characteristics of reservoirs.

Based on pyrite trace element geochemistry and lithogeochemical data, Vasilopoulos et al. (2023) suggested that ore-forming components at Hirvilavanmaa were most likely sourced from mafic metavolcanic rocks of the Kittilä suite. Combined results of tourmaline boron isotope analyses and of sulfur isotope analyses from sulfides support this conclusion. Tourmaline from Hirvilavanmaa falls in the middle range of Mid Ocean Ridge Basalts (MORB), granitoids, non-marine evaporites and clastic metasediments in terms of global boron reservoirs (Fig. 7); since granitoids are not known in the vicinity of the deposit, they can be confidently excluded. On the other hand, hydrothermal pyrite from Hirvilavanmaa has mostly $\delta^{34}S$ values close to 0‰ with a median of

+1.3‰ (Supplementary Table S1). Sulfur isotope values close to 0‰ are typical for magmatic sulfur (e.g., Ohmoto, 1986) and can also reflect leaching of sulfur from igneous rocks (e.g., Li et al., 2018). Considering the potential boron reservoirs in combination with the sulfur isotope composition of pyrite, a mafic metavolcanic rock source for ore-forming components is supported for Hirvilavanmaa in line with the model of Vasilopoulos et al. (2023). The boron isotope composition of tourmaline types I_H and II_H from Hirvilavanmaa is distinct with mean $\delta^{11}B$ values of −5.6‰ and −8.7‰, respectively (Fig. 8). A changing fluid/rock ratio can produce variations on the boron isotope composition of tourmaline through boron leaching and isotope exchange (Jiang et al., 2000; Trumbull et al., 2020). The distinct boron isotope compositions of tourmaline types I_H and II_H further support a generally low but changing fluid/rock ratio during different mineralizing stages at Hirvilavanmaa. A higher fluid/rock ratio during Type II_H tourmaline deposition meant that its boron isotope composition mostly reflects the inferred mafic metavolcanic rock source. The lower fluid/rock ratio during Type I_H deposition resulted in a stronger influence of the boron isotope composition of the ultramafic host rocks; since ultramafic rocks have a generally heavier boron isotopic signature compared to MORB (Fig. 8; Trumbull et al., 2020), a shift towards heavier values was recorded in the boron isotope composition of Type I_H tourmaline.

The sulfur isotope composition of sulfides from Naakenavaara (median +9.9‰) corresponds well with sulfur reduced from seawater sulfate during the Paleoproterozoic, being ~10‰ lighter than the seawater sulfate curve at the time, and fitting with the curve describing the variation of sulfur isotope composition in sediment-hosted orogenic deposits through time (Chang et al., 2008). This suggests a metasedimentary origin of sulfur at Naakenavaara. Black schists of the Savukoski group have pyrite with high $\delta^{34}S$ values (mostly > +10‰, mean ~ +16‰; Hanski and Huhma, 2005), making them a plausible source of sulfur for Naakenavaara. Pyrite deposited in the early Co-rich stage (Py_{Naak}-mid) has a median $\delta^{34}S$ of +8.6‰, whereas pyrite deposited in the main Cu-rich stage (Py_{Naak}-high) has a higher median of +9.6‰. These two pyrite types have similar trace element characteristics and represent two stages of evolution of the same base metal-rich mineralizing event (Vasilopoulos et al., 2023). The boron isotope composition of all analyzed tourmaline from Naakenavaara, which was deposited during the Co (type I_N) and Cu-rich stages (type II_N-b), has a narrow range (Fig. 8) suggesting that the inferred metasedimentary source of ore-forming components, including boron, remained unchanged during these stages. On the other hand, pyrite (Py_{Naak}-low) deposited during the late Au-rich stage has a distinct trace element geochemistry, indicating a different fluid composition compared to the earlier base metal-rich stages (Vasilopoulos et al., 2023). Py_{Naak}-low also has higher $\delta^{34}S$ values (median +11.4‰) and a considerably narrower $\delta^{34}S$ range compared to pyrite deposited during the earlier base metal-rich stages (Fig. 4d). As discussed previously, the late Au-rich stage took place during a later deformation event and the different chemical composition of the fluid and higher $\delta^{34}S$ values of pyrite could be explained by considering a different part of the Savukoski group stratigraphy as being the fluid source in this late stage. The narrow range of $\delta^{34}S$ values indicates that physicochemical conditions stayed relatively constant at Naakenavaara during this late mineralizing stage.

6. Summary and conclusions

This work presents new information regarding the formation history of Au-only and (atypical) polymetallic orogenic gold deposits in the Central Lapland belt (CLB). The results of our study support different sources for ore-forming components in the Au-only Hirvilavanmaa and the atypical Naakenavaara orogenic gold deposits from the CLB. Our results also provide important geochronological constraints for orogenic gold mineralization in the CLB by comparing calculated ages of mineralizing stages in the deposits to the timing of different deformational events during the Svecofennian orogeny in the CLB. Exploration for both types of deposits is ongoing in the CLB, and a better understanding of their formation history could help focus exploration targeting in the area.

At Hirvilavanmaa, the crystal chemistry of tourmaline is characterized by low Al (<6 apfu) and high Fe_{tot} + Mg values, alignment of data points along the oxydravite to povondraite trend on the AFM diagram, and an influence of the $FeAl_{-1}$ exchange indicating relatively oxidizing conditions during tourmaline deposition. Significantly elevated Cr concentrations indicate a generally low fluid/rock ratio that resulted in tourmaline being influenced by the composition of the ultramafic metavolcanic host rocks. Results of sulfur isotope analyses from sulfides combined with results of boron isotope analyses from tourmaline indicate a mafic metavolcanic rock source for ore-forming components, supporting the previously established model (Vasilopoulos et al., 2023) for the same deposit based on lithogeochemical and sulfide trace element characteristics.

At Naakenavaara, tourmaline from Co ore zones has low Al (mean < 6 apfu) concentrations, is influenced by the $FeAl_{-1}$ exchange, and mostly aligns with the oxydravite to povondraite trend on the AFM diagram. Tourmaline from Cu-rich ore zones has higher Al concentrations (mean > 6 apfu) and does not align with the oxydravite to povondraite trend. These characteristics of tourmaline from Naakenavaara support the involvement of a relatively oxidized fluid during the first Co-rich and pyrite-dominant mineralizing stage, with more reduced conditions prevailing during the subsequent pyrrhotite-dominant Cu-rich stage of ore formation. Tourmaline crystal chemistry also supports a relatively low fluid/rock ratio at Naakenavaara, similarly to Hirvilavanmaa. Based on the sulfur isotope composition of sulfides (median $\delta^{34}S$ of +9.9‰), a metasedimentary source of sulfur is indicated for both the base metal-rich and the later overprinting Au-rich mineralizing events, with black schists of the Savukoski group being a plausible source for sulfur at Naakenavaara. The relatively narrow range and higher $\delta^{34}S$ values (median $\delta^{34}S$ of +11.4‰) of pyrite deposited during the late Au-rich stage, compared to pyrite deposited during the earlier base metal-rich stages (median $\delta^{34}S$ of +9.3‰), are explained by relatively constant conditions during ore deposition and by considering a different package of metasedimentary rocks as the source, respectively.

Geochronological data in this study provide distinct age constraints for the mineralizing events distinguished based on trace element characteristics of sulfides in the two studied deposits (Vasilopoulos et al., 2023). Based on the U-Pb dating of hydrothermal xenotime and monazite from both deposits. Several episodes of fluid flow are inferred along the Sirkka Shear Zone. The first ore-related episode in the deposits took place at ca. 1.82–1.80 Ga, relatively late in the history of the Svecofennian orogenesis. This period marks the Co- and Cu-rich mineralizing stages at Naakenavaara and hydrothermal fluid flow that could mark the first episode of Au deposition at Hirvilavanmaa. Later, during the waning stages of the orogeny at ca. 1.78–1.76 Ga, Au was deposited in both deposits. Similar ages of mineralizing events (1.82–1.76 Ga) have been documented in various deposits along both the Sirkka Shear Zone and the Kiistala Shear Zone (Mänttäri, 1995; Molnár et al., 2017, 2018), making this time period particularly important in terms of ore formation in the Central Lapland belt.

Results of our geochronological study from Naakenavaara are especially important as they provide texturally well-constrained age results that support what several workers (Ranta et al., 2021; Raič et al., 2022; Vasilopoulos et al., 2021, 2023) have proposed based on mineralogical and geochemical observations: in several polymetallic Au deposits of northern Finland, classified as atypical orogenic gold deposits, early base metal deposition is followed by a late orogenic Au overprint.

CRediT authorship contribution statement

Mikael Vasilopoulos: Conceptualization, Formal analysis, Investigation, Visualization, Writing – original draft, Writing – review & editing. **Ferenc Molnár:** Conceptualization, Investigation, Supervision,

Writing – review & editing. **Jukka-Pekka Ranta:** Supervision, Writing – review & editing. **Matti Kurhila:** Investigation, Validation, Writing – review & editing. **Hugh O'Brien:** Investigation, Validation, Writing – review & editing. **Yann Lahaye:** Investigation, Validation, Writing – review & editing. **Sari Lukkari:** Investigation, Writing – review & editing. **Marko Moilanen:** Investigation, Writing – review & editing.

Declaration of competing interest

The authors declare that they have no known competing financial interests or personal relationships that could have appeared to influence the work reported in this paper.

Data availability

Data will be made available on request.

Acknowledgements

This work was financially supported by grants from the Finnish Cultural Foundation, the K.H. Renlund Foundation, the Oulu University Scholarship Foundation and the Ella and Georg Ehrnrooth Foundation. We would like to thank Robert Trumbull and an anonymous reviewer for their insightful comments that helped improve the quality of this paper.

Appendix A. Supplementary data

Supplementary data to this article can be found online at https://doi.org/10.1016/j.gexplo.2024.107419.

References

Agnico Eagle, 2023. Second quarter 2023 results. Available online at: https://s21.q4cdn.com/374334112/files/doc_downloads/ops-overview-slides/Kittila.pdf.
Bogdanova, S., Gorbatschev, R., Skridlaite, G., Soesoo, A., Taran, L., Kurlovich, D., 2015. Trans-Baltic Palaeoproterozoic correlations towards the reconstruction of supercontinent Columbia/Nuna. Precambrian Res. 259, 5–33.
Budzyn, B., Slama, J., Corfu, F., Crowley, J., Schmitz, M., Williams, M.L., Jercinovic, M. J., Kozub-Budzyn, G.A., Konečny, P., Rzepa, G., Włodek, A., 2021. TS-Mnz - a new monazite age reference material for U-Th-Pb microanalysis. Chem. Geol. 572, 120195.
Catanzaro, E.J., Champion, C.E., Garner, E.L., Maienko, G., Sappenfield, K.M., Shields, W.R., 1970. Boric acid: isotopic and assay standard reference materials. In: National Bureau Standards (US). Spec Publ 260-17 (70 pp.).
Chang, Z., Large, R.R., Maslennikov, V., 2008. Sulfur isotopes in sediment-hosted orogenic gold deposits: evidence for an early timing and a seawater sulfur source. Geology 36 (12), 971–974.
Cherniak, D.J., 2006. Pb and rare earth element diffusion in xenotime. Lithos 88, 1–14.
Cherniak, D.J., Watson, E.B., Grove, M., Harrison, T.M., 2004. Pb diffusion in monazite: a progress report on a combined RBS/SIMS study. Geochim. Cosmochim. Acta 68, 829–840.
Eilu, P., 2015. Overview on gold deposits in Finland. In: Maier, W.D., O'Brien, H., Lahtinen, R. (Eds.), Mineral Deposits of Finland. Elsevier, Amsterdam, pp. 377–403.
Eilu, P., Pankka, H., Keinänen, V., Kortelainen, V., Niiranen, T., Pulkkinen, E., 2007. Characteristics of gold mineralisation in the greenstone belts of northern Finland. Geol. Surv. Finland Spec. Pap. 44, 57–106.
Eilu, P., Niiranen, T., Hulkki, H., Nykänen, V., 2012. Kittilä Au, Cu. In: Eilu, P. (Ed.), Mineral Deposits and Metallogeny of Fennoscandia, Geol Survey Finland Spec Paper 53, pp. 314–317.
Eilu, P., Rasilainen, K., Halkoaho, T., Huovinen, I., Kärkkäinen, N., Kontoniemi, O., Lepistö, K., Niiranen, T., Sorjonen-Ward, P., 2015. Quantitative assessment of undiscovered resources in orogenic gold deposits in Finland. In: Geological Survey of Finland, Report of Investigation, vol. 216 (318 pp.).
Gilbert, S.E., Danyushevsky, L.V., Rodermann, T., Shimizu, A., Gurenko, A., Meffre, S., Thomas, H., Large, R.R., Death, D., 2014. Optimisation of laser parameters for the analysis of sulphur isotopes in sulphide minerals by laser ablation ICP-MS. J. Anal. At. Spectrom. 29, 1042–1051.
Goldfarb, R.J., Groves, D.I., 2015. Orogenic gold: common or evolving fluid and metal sources through time. Lithos 233, 2–26.
Goldfarb, R.J., Pitcairn, I., 2022. Orogenic gold: is a genetic association with magmatism realistic? Mineral. Deposita. https://doi.org/10.1007/s00126-022-01146-8.
Goldfarb, R.J., Baker, T., Dube, B., et al., 2005. Distribution, character, and genesis of gold deposits in metamorphic terranes. In: Econ Geol 100th Anniversary Vol, pp. 407–450.
Gonçalves, G.O., Lana, C., Scholz, R., Buick, I.S., Gerdes, A., Kamo, S.L., Corfu, F., Marinho, M.M., Chaves, A.O., Valeriano, C., Nalini, H.A., 2016. An assessment of monazite from the Itambé pegmatite district for use as U-Pb isotope reference material for microanalysis and implications for the origin of the "Moacyr" monazite. Chem. Geol. 424, 30–50.
Groves, D., Goldfarb, R.J., Hart, C., 2003. Gold deposits in metamorphic belts: overview of current understanding, outstanding problems, future research, and exploration significance. Econ. Geol. 98, 1–29.
Groves, D.I., Santosh, M., Deng, J., Qingfei, W., Yang, L., Zhang, L., 2020. A holistic model for the origin of orogenic gold deposits and its implications for exploration. Mineral. Deposita 55, 275–292.
GTK, 2023. Mineral deposits and exploration database. Available at: https://gtkdata.gtk.fi/mdae/index.html.
Hanski, E., Huhma, H., 2005. Central Lapland greenstone belt. In: Lehtinen, M., Nurmi, P.A., Rämö, O.T. (Eds.), Precambrian Bedrock of Finland—Key to the Evolution of the Fennoscandian Shield. Elsevier, Amsterdam, pp. 139–193. https://doi.org/10.1016/S0166-2635(05)80005-2.
Hazarika, P., Mishra, B., Pruseth, K.L., 2015. Diverse tourmaline compositions from orogenic gold deposits in the Hutti-Maski greenstone belt, India: implications for sources of ore-forming fluids. Econ. Geol. 110, 337–353.
Henry, D.J., Dutrow, B.L., 2012. Tourmaline at diagenetic to low-grade metamorphic conditions: Its petrologic applicability. Lithos 154, 16–32.
Henry, D.J., Dutrow, B.L., 1996. Metamorphic tourmaline and its petrologic applications. In: Anovitz, L.M., Grew, E.S. (Eds.), Boron: Mineralogy, Petrology and Geochemistry, vol. 33, pp. 503–557.
Henry, D.J., Guidotti, C.V., 1985. Tourmaline as a petrogenetic indicator mineral: an example from the staurolite-grade metapelites of NW Maine. Am. Mineral. 70, 1–15.
Henry, D.J., Sun, H., Slack, J.F., Dutrow, B.L., 2008. Tourmaline in metaevaporites and highly magnesian rocks: perspectives from Namibian tourmalinites. Eur. J. Mineral. 20, 889–904.
Hetherington, C.J., Harlov, D.E., 2008. Metasomatic thorite and uraninite inclusions in xenotime and monazite from granitic pegmatites, Hidra anorthosite massif, southwestern Norway: mechanics and fluid chemistry. Am. Mineral. 93, 806–820.
Hetherington, C.J., Harlov, D.E., Budzyń, B., 2010. Experimental metasomatism of monazite and xenotime: mineral stability, REE mobility and fluid composition. Mineral. Petrol. 99, 165–184.
Hodkiewicz, P.F., Groves, D.I., Davidson, G.J., Weinberg, R.F., Hagemann, S.G., 2009. Influence of structural setting on sulphur isotopes in Archaean orogenic gold deposits, eastern Goldfields Province, Yilgran, Western Australia. Mineral. Deposita 44, 129–150.
Holma, M.J., Keinänen, V.J., 2007. The Levijärvi-Loukinen gold occurrence: an example of orogenic gold mineralisation with atypical metal association. In: Ojala, V.J. (Ed.), Gold in the Central Lapland Greenstone Belt, Finland, Geol Survey Finland, Spec Paper 44, pp. 165–184.
Holma, M.J., Eilu, P., Keinänen, V.J., Ojala, V.J., 2007. The Sirkka Au-Cu-Ni-Co occurrence, northern Finland: an orogenic gold deposit with multimetallic, atypical metal association. In: Andrew, C.J., et al. (Eds.), Digging Deeper, Proceedings of the Ninth Biennial SGA Meeting, Dublin, pp. 581–584.
Hölttä, P., Heilimo, E., 2017. Metamorphic map of Finland. In: Nironen, M. (Ed.), Geol Survey Finland Spec Paper 60, pp. 77–128.
Hölttä, P., Huhma, H., Mänttäri, I., Paavola, J., 2000. P-T-t development of Archaean granulites in Varpaisjarvi, Central Finland, II: dating of high-grade metamorphism with the U-Pb and Sm-Nd methods. Lithos 50, 121–136.
Hölttä, P., Väisänen, M., Väänänen, J., Manninen, T., 2007. Paleoproterozoic metamorphism and deformation in central Finnish Lapland. Geol. Surv. Finland Spec. Pap. 44, 109–120.
Hou, K.J., Li, Y.H., Liu, F., Tian, Y.R., 2010. In situ Boron isotope measurements of natural geological materials by LA-MC-ICP-MS. Chin. Sci. Bull. 55, 3305–3311.
Hulkki, H., Keinänen, V., 2007. The alteration and fluid inclusion characteristics of the Hirvilavanmaa gold deposit, Central Lapland Greenstone Belt, Finland. In: Geological Survey of Finland, Special Paper 44, pp. 137–153.
Hutchison, W., Finch, A.A., Boyce, A.J., 2020. The sulfur isotope evolution of magmatic-hydrothermal fluids: insights into ore-forming processes. Geochim. Cosmochim. Acta 288, 176–198.
Jiang, S.-Y., Palmer, M.R., Slack, J.F., Anderson, D., 2000. Chemical and boron isotopic compositions of tourmaline from massive sulphide deposits and tourmalinites in the Mesoproterozoic Belt and Purcell supergroups, southeastern British Columbia and northwestern Montana. In: Lydon, J.W., Höy, T., Slack, J.F., Knapp, M.E. (Eds.), Geological Environment of the Sullivan Deposit, British Columbia, Geol. Assoc. Canada, Mineral Deposits Div. Spec. Publ. 1, pp. 336–354.
Jiang, S.-Y., Palmer, M.R., Yeats, C.J., 2002. Chemical and boron isotopic compositions of tourmaline from the Archean Big Bell and Mount Gibson gold deposits, Murchison Province, Yilgarn craton, Western Australia. Chem. Geol. 188, 229–247.
Keinänen, V., 2002. Tutkimustyöselostus Kittilän kunnassa valtausalueilla Naakenavaara 1, Kaiv. Rek.N:O 5522/1, Naakenavaara 2, Kaiv. Rek.N:O 5522/2, Naakenavaara 3, Kaiv. Rek. N:O 6089/3, Naakenavaara 4 ja 5, Kaiv. Rek.N:ROT 6159/1 ja 2, Naakenavuoma 1 ja 2, Kaiv.Rek.N:Rot 6089/1 ja 2 sekä Puutanperä 1, Kaiv.Rek.N:O 5686/1 suoritetuista malmitutkimuksista. In: Geol Survey Finland Claim Report M06/2734/2002/1/10 (6 pp.).
Keith, M., Smith, D.J., Jenkin, G.R.T., Holwell, D.A., Rye, M.D., 2018. A review of Te and Se systematics in hydrothermal pyrite from precious metal deposits: insights into ore-forming processes. Ore Geol. Rev. 96, 269–282.
Korja, A., Lahtinen, R., Nironen, M., 2006. The Svecofennian orogen: a collage of microcontinents and island arcs. In: Gee, D.G., Stephenson, R.A. (Eds.), European Lithosphere Dynamics, Geological Society, London, Memoirs, pp. 561–578.
Köykkä, J., Lahtinen, R., Huhma, H., 2019. Provenance evolution of the Paleoproterozoic metasedimentary cover sequences in northern Fennoscandia: age distribution, geochemistry, and zircon morphology. Precambrian Res. 331, 105364.

Lahtinen, R., Korja, A., Nironen, M., 2005. Paleoproterozoic tectonic evolution. In: Lehtinen, M., Nurmi, P.A., Rämö, O.T. (Eds.), Precambrian Geology of Finland: Key to the Evolution of the Fennoscandian Shield. Elsevier, Amsterdam, pp. 481–532.
Lahtinen, R., Hallberg, A., Korsakova, M., Sandstad, J.S., Eilu, P., 2012. Main metallogenic events in Fennoscandia. In: Geol Surv Finl Spec Pap 53, pp. 397–401.
Lahtinen, R., Sayab, M., Karell, F., 2015. Near-orthogonal deformation successions in the poly-deformed Paleoproterozoic Martimo Belt: implications for the tectonic evolution of northern Fennoscandia. Precambrian Res. 270, 22–38. https://doi.org/10.1016/j.precamres.2015.09.003.
Lehtonen, M.I., Airo, M.-L., Eilu, P., Hanski, E., Kortelainen, V., Lanne, E., Manninen, T., Rastas, P., Räsänen, J., Virransalo, P., 1998. Kittilän vihreäkivialueen geologia. Lapin vulkaniittiprojektin raportti. Summary: the stratigraphy, petrology and geochemistry of the Kittilä greenstone area, northern Finland. A report of the Lapland Volcanite Project. In: Geol Survey Finland, Report of Investigation, vol. 140 (144 pp.).
Li, R., Chen, H., Xia, X., Yang, Q., Danyushevsky, L.V., Lai, C., 2018. Using integrated in-situ sulfide trace element geochemistry and sulfur isotopes to trace ore-forming fluids: example from the Mina Justa IOCG deposit (southern Perú). Ore Geol. Rev. 101, 165–179.
Ludwig, K.R., 2012. Users manual for ISOPLOT/EX, Version 3. A geochronological toolkit for Microsoft Excel. In: Berkeley Geochronological Centre Special Publication.
Mänttäri, I., 1995. Lead isotope characteristics of epigenetic gold mineralization in the Palaeoproterozoic Lapland greenstone belt, northern Finland. Bulletin 381 (70 pp.).
Marschall, H.R., Jiang, S.-Y., 2011. Tourmaline isotopes: no element left behind. Elements 7, 313–319.
Molnár, F., Mänttäri, I., O'Brien, H., Lahaye, Y., Pakkanen, L., Johanson, B., Käpyaho, A., Sorjonen-Ward, P., Whitehouse, M., Sakellaris, G., 2016. Boron, sulphur and copper isotope systematics in the orogenic gold deposits of the Archean Hattu schist belt, eastern Finland. Ore Geol. Rev. 77, 133–162.
Molnár, F., O'Brien, H., Lahaye, Y., Kurhila, M., Middleton, A., Johanson, B., 2017. Multi-stage hydrothermal processes and diverse metal associations in orogenic gold deposits of the Central Lapland Greenstone Belt, Finland. In: Mineral Resources to Discover–14th SGA Biennial Meeting, pp. 63–66.
Molnár, F., Middleton, A., Stein, H., O'Brien, H., Lahaye, Y., Huhma, H., Pakkanen, L., Johanson, B., 2018. Repeated syn- and post- orogenic gold mineralization events between 1.92 and 1.76 along the Kiistala Shear Zone in the Central Lapland Greenstone Belt, northern Finland. Ore Geol. Rev. 101, 936–959.
Molnár, F., Lahaye, Y., O'Brien, H., Kurhila, M., Hulkki, H., 2019. The Saattopora orogenic Au-Cu deposit, Central Lapland Greenstone belt, Finland: fluid sources and timing of hydrothermal processes. In: Life With Ore Deposits on Earth–15th SGA Biennial Meeting, pp. 723–726.
Müller, W., Shelley, M., Miller, P., Broude, S., 2009. Initial performance metrics of a new custom-designed ArF excimer LA-ICPMS system coupled to a two-volume laser-ablation cell. J. Anal. At. Spectrom. 24, 209–214.
Nenonen, E., 1975. Selostus Kittilän Riikonkosken ympäristön malminetsintätöistä vuosilta 1971–1974. In: Geol Survey Finland Claim Report M19/2734/-75/1 (30 pp.).
Niiranen, T., Lahti, I., Nykänen, V., 2015. Chapter 10.2 – the orogenic gold potential of the Central Lapland Greenstone Belt, Northern Fennoscandian Shield. In: Maier, W. D., Lahtinen, R., O'Brien, H. (Eds.), Mineral Deposits of Finland. Elsevier, Amsterdam, pp. 733–752.
Nironen, M., 2005. Proterozoic orogenic granitoid rocks. In: Lehtinen, M., Nurmi, P.A., Rämö, O.T. (Eds.), Precambrian Geology of Finland–Key to the Evolution of the Fennoscandian Shield. Elsevier, Amsterdam, pp. 443–480.
Ohmoto, H., 1972. Systematics of sulfur and carbon isotopes in hydrothermal ore deposits. Econ. Geol. 67, 551–578.
Ohmoto, H., 1986. Stable isotope geochemistry of ore deposits. In: Valley, J.W., Taylor Jr., H.P., O'Neil, J.R. (Eds.), Stable Isotopes in High Temperature Geological Processes, Rev Mineralogy 16, pp. 491–559.
Ohmoto, H., Rye, R.O., 1979. Isotopes of sulfur and carbon. In: Barnes, H.L. (Ed.), Geochemistry of Hydrothermal Ore Deposits. J Wiley and Sons, pp. 509–567.
Pajunen, M., Poutiainen, M., 1999. Palaeoproterozoic prograde metasomatic-metamorphic overprint zones in Archaean tonalitic gneisses, eastern Finland. Bull. Geol. Soc. Finl. 71, 73–132.
Palmer, M.R., Swihart, G.H., 1996. Boron isotope geochemistry: an overview. In: Grew, E.S., Anovitz, L.M. (Eds.), Boron: Mineralogy, Petrology, and Geochemistry, Rev Mineral 33, pp. 709–744.
Patison, N.L., 2007. Structural controls on gold mineralisation in the Central Lapland Greenstone Belt. In: Geol Survey Finland, Spec Paper 44, pp. 107–124.
Patten, C.G.C., Pitcairn, I.K., Molnár, F., Kolb, J., Beaudoin, G., Guilmette, C., Peillod, A., 2020. Gold mobilization during metamorphic devolatilization of Archean and Paleoproterozoic metavolcanic rocks. Geology 48 (11), 1110–1114.
Patten, C.G.C., Molnár, F., Pitcairn, I.K., Kolb, J., Mertanen, S., Hector, S., 2023. Multi-source and multi-stage metal mobilization during the tectonic evolution of the Central Lapland Greenstone Belt, Finland: implications for the formation of orogenic Au deposits. Mineral. Deposita 58, 461–488.
Phillips, G.N., Powell, R., 2010. Formation of gold deposits—a metamorphic devolatilization model. J. Metamorph. Geol. 28, 689–718.
Pitcairn, I.K., Leventis, N., Beaudoin, G., Faure, S., Guilmette, C., Dubé, B., 2021. A metasedimentary source of gold in Archean orogenic gold deposits. Geology 49, 862–866.
Qiu, Z.-J., Fan, H.-R., Goldfarb, R., Tomkins, A.G., Yang, K.-F., Li, X.-C., Xie, L.-W., Liu, X., 2021. Cobalt concentration in a sulfidic sea and mobilization during orogenesis: implications for targeting epigenetic sediment-hosted Cu-Co deposits. Geochim. Cosmochim. Acta 305, 1–18.
Raič, S., Molnár, F., Cook, N., O'Brien, H., Lahaye, Y., 2022. Application of lithogeochemical and pyrite trace element data for the determination of vectors to ore in the Raja Au-Co prospect, northern Finland. Solid Earth 13, 271–299.
Ranta, J.-P., Hanski, E., Cook, Ni, Lahaye, Y., 2017. Source of boron in the Palokas gold deposit, northern Finland: evidence from boron isotopes and major element composition of tourmaline. Mineral. Deposita 52, 733–746.
Ranta, J.-P., Cook, N., Gilbricht, S., 2021. SEM-based automated mineralogy (SEM-AM) and unsupervised machine learning studying the textural setting and elemental association of gold in the Rajapalot Au-Co area, northern Finland. Bull. Geol. Soc. Finl. 93, 129–154.
Rasmussen, B., Fletcher, I.R., Muhling, J.R., 2011. Response of xenotime to prograde metamorphism. Contrib. Mineral. Petrol. 162, 1259–1277.
Rupert Resources, 2020. Media release, 16 March 2020. Available online at: http://tupa.gtk.fi/karttasovellus/mdae/references/390_Hirvilavanmaa/390_Rupert043_20200316.pdf.
Salli, I., 1983. Pielavesi. Explanation to the Geological map of Finland 1:100000, pre-Quaternary rocks, sheet 3314. In: Geological Survey of Finland (29 pp.).
Sayab, M., Molnár, F., Aerden, D., Niiranen, T., Kuva, J., Välimaa, J., 2020. A succession of near-orthogonal horizontal tectonic shortenings in the Paleoproterozoic Central Lapland Greenstone Belt of Fennoscandia: constrains from the world-class Suurikuusikko gold deposit. Mineral. Deposita. https://doi.org/10.1007/s00126-019-00910-7.
Sayab, M., Lahtinen, R., Köykkä, J., Hölttä, P., Katinen, T., Niiranen, T., Leväniemi, H., 2021. Improved resolution of Paleoproterozoic orogenesis: multi-directional collision tectonics in the Sodankylä belt of northern Finland. Precambrian Res. 359, 106193.
Sciuba, M., Beaudoin, G., Makvandi, S., 2021. Chemical composition of tourmaline in orogenic gold deposits. Mineral. Deposita 56, 537–560.
Seal, R.R., 2006. Sulfur isotope geochemistry of sulfide minerals. Rev. Mineral. Geochem. 61, 633–677.
Seydoux-Guillaume, A.-M., Montel, J.-M., Bingen, B., Bosse, V., de Parseval, P., Paquette, J.-L., Janots, E., Wirth, R., 2012. Low-temperature alteration of monazite: fluid mediated coupled dissolution–precipitation, irradiation damage, and disturbance of the U-Pb and Th–Pb chronometers. Chem. Geol. 330–331, 140–158.
Slack, J.F., Coad, P.R., 1989. Multiple hydrothermal and metamorphic events in the Kidd Creek volcanogenic massive sulphide deposit, Timmins, Ontario: evidence from tourmalines and chlorites. Can. J. Earth Sci. 26 (4), 694–715.
Stacey, J.S., Kramers, J.D., 1975. Approximation of terrestrial lead isotope evolution by a two-stage model. Earth Planet. Sci. Lett. 26, 207–221.
Tajcmanová, L., Soejono, I., Konopásek, J., Kosler, J., Klötzli, U., 2010. Structural position of high-pressure felsic to intermediate granulites from NE Moldanubian domain (Bohemian Massif). J. Geol. Soc. Lond. 167, 329–345.
Taranis Resources, 2010. Press release 24/11/2010. Available online at: http://tupa.gtk.fi/karttasovellus/mdae/references/437_Naakenavaara/437_Taranis_PressRelease_2010_11_24.pdf.
Taranis Resources, 2011. Press release 12/9/2011. Available online at: http://tupa.gtk.fi/karttasovellus/mdae/references/437_Naakenavaara/437_Taranis_PressRelease_2011_09_12.pdf.
Taranis Resources, 2014. Taranis Resources Inc. management discussion & analysis, for the year ended December 31, 2013 (including subsequent events to April 15, 2014). Available online at: http://tupa.gtk.fi/karttasovellus/mdae/references/437_Naakenavaara/437_Taranis_2013_Annual_MD&A.pdf.
Tonarini, S., Pennisi, M., Adorni Braccesi, A., Dini, A., Ferrara, G., Confiantini, R., Wiedenbeck, M., Gröning, M., 2003. Intercomparison of boron isotope concentration measurements. Part I: selection, preparation and homogeneity tests of the intercomparison materials. Geostand. Newslett. 27, 21–39.
Trumbull, R.B., Codeço, M.S., Jiang, S.-Y., Palmer, M.R., Slack, J.F., 2020. Boron isotope variations in tourmaline from hydrothermal ore deposits: a review of controlling factors and insights for mineralizing systems. Ore Geol. Rev. 125, 103682.
van Achterberg, E., Ryan, C., Jackson, S., Griffin, W., 2001. Data reduction software for LA-ICP-MS. In: Sylverster, P. (Ed.), Laser-Ablation ICPMS in the Earth Sciences–Principles and Applications, Mineralogical Association of Canada Short Course Series, vol. 29, pp. 239–243. St John, Newfoundland.
van Hinsberg, V.J., Henry, D.J., Marschall, H.R., 2011. Tourmaline: an ideal indicator of its environment. Can. Mineral. 49, 1–16.
Vasilopoulos, M., Molnár, F., O'Brien, H., Lahaye, Y., Lefèbvre, M., Richard, A., André-Mayer, A.-S., Ranta, J.-P., Talikka, M., 2021. Geochemical signatures of mineralizing events in the Juomasuo Au–Co deposit, Kuusamo belt, northeastern Finland. Mineral. Deposita 56, 1195–1222.
Vasilopoulos, M., Molnár, F., Ranta, J.-P., O'Brien, H., 2023. Mineralogical, lithogeochemical and sulfide trace element characteristics of the Hirvilavanmaa Au-only and the base metal-rich Naakenavaara orogenic gold deposits in the Central Lapland belt, northern Finland. J. Geochem. Explor. 244, 107132.
Vermeesch, P., 2018. IsoplotR: a free and open toolbox for geochronology. Geosci. Front. 9, 1479–1493.
Vielreicher, N.M., Groves, D.I., McNaughton, N.J., Fletcher, I.R., 2015. The timing of gold mineralization across the eastern Yilgarn craton using U-Pb geochronology of hydrothermal phosphate minerals. Mineral. Deposita 50, 391–428.
Williams, M.L., Jercinovic, M.J., Harlov, D.E., Budzyń, B., Hetherington, C.J., 2001. Resetting monazite ages during fluid-related alteration. Chem. Geol. 283, 218–225.
Wyche, N.L., Eilu, P., Koppström, K., Kortelainen, V.J., Niiranen, T., Välimaa, J., 2015. Chapter 5.2 – the Suurikuusikko gold deposit (KittilÄ Mine), Northern Finland. In: Maier, Wolfgang D., Lahtinen, Raimo, O'Brien, Hugh (Eds.), Mineral Deposits of Finland. Elsevier, Amsterdam, pp. 411–433.
Yardley, B.W.D., Cleverley, J.S., 2013. The role of metamorphic fluids in the formation of ore deposits. Geol. Soc. London Spec. Publ. 393 https://doi.org/10.1144/SP393.5.

Yardley, B.W.D., Graham, J.T., 2002. The origins of salinity in metamorphic fluids. Geofluids 2, 249–256.
Yavuz, F., Karakaya, N., Yildirim, D.K., Karakaya, M.C., Kumral, M., 2011. A Windows program for calculation and classification of tourmaline-supergroup (IMA-2011). Comput. Geosci. 63, 70–87.
Zhong, R., Brugger, J., Tomkins, A.G., Chen, Y., Li, W., 2015. Fate of gold and base metals during metamorphic devolatilization of a pelite. Geochim. Cosmochim. Acta 171, 338–352.